Supporting Information for

Poly(vinylphenoxazine) as Fast-Charging Cathode Material for Organic Batteries

Fabian Otteny,[1,6] Verena Perner,[2,6] Daniel Wassy,[1] Martin Kolek,[2,*] Peter Bieker,[2] Martin Winter[2,3] and Birgit Esser[1,4,5,7,*]

[1] Institute for Organic Chemistry, University of Freiburg, Albertstraße 21, 79104 Freiburg, Germany

[2] MEET Battery Research Center, Institute of Physical Chemistry, University of Münster, Corrensstraße 46, 48149 Münster, Germany

[3] Helmholtz-Institute Münster (HI MS), IEK-12, Forschungszentrum Jülich GmbH, Corrensstrasse 46, 48149 Münster, Germany

[4] Freiburg Materials Research Center, University of Freiburg, Stefan-Meier-Straße 19, 79104 Freiburg, Germany

[5] Cluster of Excellence livMatS @ FIT – Freiburg Center for Interactive Materials and Bioinspired Technologies, University of Freiburg, Georges-Köhler-Allee 105, 79110 Freiburg, Germany

[6] These authors contributed equally

[7] Lead contact

* Correspondence: besser@oc.uni-freiburg.de, martin.kolek@uni-muenster.de

Number of pages: 47

Number of figures: 36

Number of tables: 8

Contents

1 Synthesis and characterization data of PVMPO and X-PVMPO

1.1 Materials and methods

Commercially available chemicals were purchased from ACROS, CHEMPUR, FISHER CHEMICAL and SIGMA-ALDRICH and used without further purification unless otherwise noted. Solvents purchased in technical grade were distilled prior to use, analytical grade solvents were used as received. Anhydrous solvents were obtained from an M. BRAUN solvent purification system (*MB-SPS-800*) and stored over molecular sieves (3 Å) for a minimum duration of 72 h. Air- and moisture-sensitive reactions were carried out under an argon atmosphere in glassware dried by heating under vacuum using standard Schlenk techniques (Argon 5.0 from SAUERSTOFFWERK FRIEDRICHSHAFEN).

Analytical thin layer chromatography was carried out by using silica gel-coated aluminium plates with a fluorescence indicator (MERCK *60 F_{254}*). Detection was carried out by using short-wave UV light (λ_{max} = 254 nm). Flash column chromatography was carried out by using silica gel *Silica 60* (grain size 40–63 µm, 230–400 mesh) from MACHERY-NAGEL.

NMR spectra were recorded on BRUKER *Avance III HD* (^{1}H = 500 MHz, ^{13}C = 125 MHz), BRUKER *Avance II* (^{1}H = 400 MHz, ^{13}C = 100 MHz) and BRUKER *Avance III HD* (^{1}H = 300 MHz) spectrometers in deuterated solvent solution at 298 K. Chemical shifts are reported in parts per million (ppm, δ scale) and are referenced to the residual solvent signal ($CDCl_3$: δ_H 7.26 ppm, δ_C = 77.16 ppm). Analysis followed first order and data are presented as follows: chemical shift, multiplicity (s = singlet, d = doublet, dd = doublet of doublet, ddd = doublet of doublet of doublet, m = multiplet), coupling constants (*J*) in Hertz [Hz] and integration.

HRMS spectra were measured on a THERMO FISHER SCIENTIFIC *Exactive* spectrometer with orbitrap analyzer. For ionization APCI and ESI were used.

GC/MS spectra were measured on a THERMO SCIENTIFIC *TRACE 1300 Gas Chromatograph* combined with an *ISQ LT Single Quadrupole Mass Spectrometer* using electron impact ionization (EI).

FT-IR measurements were performed on a THERMO FISHER SCIENTIFIC *Nicolet iS10* spectrometer equipped with a diamond-ATR module. Spectra were recorded at 298 K in the range of 4000–550 cm^{-1} with a resolution of 2 cm^{-1} and averaged over 64 scans. The THERMO FISHER SCIENTIFIC software *OMNIC* was used for acquiring data. All spectra were normalized to 1 and intensities are given as follows: vw = very weak (< 0.2), w = weak (< 0.4), m = medium (< 0.6), s = strong (< 0.8), vs = very strong (≥ 0.8).

UV/Vis/NIR absorption spectra were measured with a *Lambda 950* spectrometer from PERKINELMER using sealable *Quartz Suprasil* cuvettes from HELLMA ANALYTICS.

Elemental analysis was performed on an ELEMENTAR *vario MICRO cube* using a thermal conductivity detector (TCD).

GPC was performed on a *SECcurity GPC System* from PSS POLYMER STANDARDS SERVICE using components of the *1260 Infinity* series from AGILENT TECHNOLOGIES. Measurements in THF were performed at 35 °C with a flow rate of 1 mL min^{-1} and a set of three columns (PSS SDV, 8 mm × 50 mm pre-column, 8 mm × 300 mm columns with a porosity of 1.000 Å and 100.000 Å). For calibration, polystyrene standards by PSS were used.

TGA (thermogravimetric analysis) was performed on a NETZSCH *STA 409 C* and **DSC** (differential scanning calorimetry) on a NETZSCH *DSC 204 F1 Phoenix*. Evaluation of the data was perfomed with *Proteus Thermal Analysis* by NETZSCH.

Spectroelectrochemistry was performed using a combination of a *VersaSTAT 4* potentiostat by PRINCETON APPLIED RESEARCH and a *SPECORD S 300 VIS* spectrometer by ANALYTIK JENA. Measurements were carried out in anhydrous dichloromethane (10 mM of analyte, referenced to the amount of redox-active subunits) containing *n*-Bu_4NPF_6 (0.2 M) as supporting electrolyte. As working electrode (WE) a platinum net was used, as counter electrode (CE) a platinum rod and as reference electrode (RE) a $Ag/AgNO_3$ electrode containing a silver wire immersed in an inner chamber filled with $AgNO_3$ (0.01 M) and *n*-Bu_4NPF_6 (0.1 M) in anhydrous acetonitrile. To apply the desired potential a chronoamperometric measurement was performed using the software *VersaStudio* to adjust the parameters. UV/Vis spectra were recorded at an interval of 30 seconds using the software *WinASPECT*.

1.2 Synthesis of PVMPO and X-PVMPO

1.2.1 Synthesis of *N*-methylphenoxazine (MPO)

A solution of phenoxazine (**1**, 1.00 g, 5.46 mmol) in dry THF (20 mL) was added to a solution of potassium *tert*-butoxide (919 mg, 8.19 mmol) in dry THF (30 mL) at 0 °C. After stirring for 1 h, methyl iodide (0.68 mL, 10.9 mmol) was added to the solution. The mixture was stirred at room temperature for 42 h. The reaction was quenched with water (20 mL), and the resulting mixture was extracted with ethyl acetate (3 × 50 mL). The combined organic layers were washed with water and brine, dried over $MgSO_4$, filtered and evaporated to dryness under reduced pressure. Column chromatography (silica gel, cyclohexane/ethyl acetate: 10/1) afforded *N*-methylphenoxazine (**MPO**, 1.05 g, 5.35 mmol, 98%) as a colorless oil. R_f 0.59 (cyclohexane/ethyl acetate: 10/1); ^{1}H NMR (300 MHz, $CDCl_3$): δ 6.90–6.82 (m, 2H), 6.73–6.67 (m, 4H), 6.53 (d, *J* = 7.7 Hz, 2H), 3.05 (s, 3H); ^{13}C NMR (100 MHz, $CDCl_3$): δ 145.8, 135.2, 123.9, 121.1, 115.4, 111.5, 31.0; HRMS (ESI+): *m/z* calcd. for $C_{13}H_{11}NO$ 197.0835 $[M]^+$, found 197.0835.

1.2.2 Synthesis of *N*-methylphenoxazinyl-3-carbaldehyde (2)

Phosphoryl chloride ($POCl_3$, 0.42 mL, 4.46 mmol) was added dropwise to dry DMF (1.50 mL, 19.5 mmol) at 0 °C. A solution of *N*-methylphenoxazine (**MPO**, 800 mg, 4.06 mmol) in dry 1,2-dichloroethane (9 ml) was added dropwise, and the reaction mixture was stirred at 0 °C for 1 h, warmed to room temperature and then stirred for 24 h at 90 °C. After cooling to room temperature, saturated aq. NaOAc solution (20 mL) was added. The aqueous layer was extracted with dichloromethane (3 × 50 mL). The combined organic layers were washed with water and brine, dried over $MgSO_4$, filtered and evaporated to dryness under reduced pressure. Column chromatography (silica gel, cyclohexane/ethyl acetate: 4/1) afforded *N*-methylphenoxazinyl-3-carbaldehyde (**2**, 824 mg, 3.66 mmol, 90%) as a yellow solid. R_f 0.47 (cyclohexane/ethyl acetate: 2/1); ^{1}H NMR (400 MHz, $CDCl_3$): δ 9.69 (s, 1H), 7.35 (dd, *J* = 8.2, 1.9 Hz, 1H), 7.13 (d, *J* = 1.8 Hz, 1H), 6.87 (ddd, *J* = 7.9, 7.4, 1.6 Hz, 1H), 6.77 (ddd, *J* = 7.9, 7.8, 1.6 Hz, 1H), 6.71 (dd, *J* = 7.8, 1.6 Hz, 1H), 6.57 (dd, *J* = 7.8, 1.6 Hz, 1H), 6.55 (d, *J* = 7.9 Hz, 1H), 3.11 (s, 3H); ^{13}C NMR (100 MHz, $CDCl_3$): δ 189.9, 145.8, 145.2, 140.8, 133.1, 130.3, 128.8, 124.2, 122.7, 115.8, 114.3, 112.3, 110.9, 31.4; HRMS (APCI+): *m/z* calcd. for $C_{14}H_{12}NO_2$ 226.0863 $[M+H]^+$, found 226.0865.

1.2.3 Synthesis of 3-vinyl-*N*-methylphenoxazine (3)

Methyltriphenylphosphonium bromide (2.08 g, 5.83 mmol) was added to a solution of potassium *tert*-butoxide (747 mg, 6.66 mmol) in dry THF (15 mL), and the solution was stirred at room temperature for 40 min. *N*-Methylphenoxazinyl-3-carbaldehyde (**2**, 721 mg, 3.20 mmol) was added to the solution, and the reaction mixture was stirred at room temperature for 24 h. The reaction was quenched with water (10 mL) and extracted with ethyl acetate (3 × 100 mL). The combined organic extracts were dried

over $MgSO_4$, filtered, and the solvent was removed under reduced pressure. Column chromatography (silica gel, cyclohexane/ethyl acetate: 8/1 to 1/1) yielded 3-vinyl-*N*-methylphenoxazine (**3**, 697 mg, 3.12 mmol, 98%) as a yellow solid. R_f 0.60 (cyclohexane/ethyl acetate: 5/1); ^{1}H NMR (500 MHz, $CDCl_3$): δ 6.88–6.83 (m, 2H), 6.82 (d, *J* = 2.0 Hz, 1H), 6.73–6.69 (m, 2H), 6.54 (dd, *J* = 17.5, 10.8 Hz, 1H), 6.53 (d, *J* = 7.9 Hz, 1H), 6.46 (d, *J* = 8.1 Hz, 1H), 5.55 (dd, *J* = 17.5, 0.9 Hz, 1H), 5.09 (dd, *J* = 10.8, 0.9 Hz, 1H), 3.05 (s, 3H); ^{13}C NMR (125 MHz, $CDCl_3$): δ 145.7, 145.5, 135.9, 134.7, 134.6, 131.1, 123.9, 122.7, 121.2, 115.5, 112.3, 111.6, 111.5, 111.2, 31.1; HRMS (ESI+): *m/z* calcd. for $C_{15}H_{13}NO$ 223.0992 $[M]^+$, found 223.0997.

1.2.4 Synthesis of poly(3-vinyl-*N*-methylphenoxazine) (PVMPO)

A solution of azobisisobutyronitrile (2.4 mg, 14 µmol) in dry and degassed THF (0.2 mL) was added to a stirred solution of 3-vinyl-*N*-methylphenoxazine (**3**, 320 mg, 1.43 mmol) in dry and degassed THF (1.2 mL). The flask was immediately immersed in a pre-heated oil bath, and the solution was stirred at 60 °C for 3 d. The reaction was quenched by adding methanol (2 mL), and the solvent was removed under reduced pressure. The residue was dissolved in CH_2Cl_2, and the polymer was precipitated from cyclohexane and cold acetone to afford **PVMPO** (245 mg, 77%) as an off-white solid. ^{1}H NMR (300 MHz, $CDCl_3$): δ 6.88 – 5.84 (m, 7H), 2.96 – 2.47 (m, 3H), 2.09 – 1.61 (m, 1H), 1.51 – 0.97 (m, 2H); FT-IR (ATR): $\tilde{\nu}_{max}$ = 627 (w), 735 (vs), 801 (m), 848 (w), 1143 (w), 1212 (m), 1272 (vs), 1360 (m), 1430 (w), 1489 (vs), 1598 (w), 2920 (vw) cm^{-1}; UV/Vis (CH_2Cl_2): λ_{max} (log ε) = 326 nm (4.00); elemental analysis: calcd (%) for $C_{15}H_{13}NO$: C 80.69, H 5.87, N 6.27; found: C 79.96, H 6.19, N 6.10; GPC (eluent THF, polystyrene standard): M_n 2.4 × 10^4 g mol^{-1}, M_w/M_n 1.7; TGA (10 °C min^{-1}, air): onset decomposition 390 °C, $T_{d10\%}$ (temperature for 10% weight loss) 392 °C; DSC (10 °C min^{-1}, air): T_g 178 °C.

1.2.5 Synthesis of 3,7-dibromo-*N*-methylphenoxazine (5)

N-Bromosuccinimide (270 mg, 1.52 mmol) was added in two portions to a solution of *N*-methyl-phenoxazine (**MPO**, 130 mg, 0.66 mmol) in dry dichloromethane (4 mL) at 0 °C. After warming to room temperature, the solution was stirred for 16 h. The reaction was quenched by adding water and a saturated aqueous solution of Na_2CO_3 (10 mL). The aqueous layer was extracted with dichloromethane (3 × 15 mL). The combined organic extracts were dried over $MgSO_4$, filtered, and the solvent was removed under reduced pressure. Column chromatography (silica gel, cyclohexane/ethyl acetate: 10/1) yielded 3,7-dibromo-*N*-methylphenoxazine (**5**, 210 mg, 0.59 mmol, 90%) as a white solid. R_f 0.36 (cyclohexane/ethyl acetate: 10/1); ^{1}H NMR (500 MHz, $CDCl_3$): δ 6.95 (dd, *J* = 8.5, 2.2 Hz, 2H), 6.80 (d, *J* = 2.3 Hz, 2H), 6.35 (d, *J* = 8.5 Hz, 2H), 2.98 (s, 3H); ^{13}C NMR (125 MHz, $CDCl_3$): δ 145.8, 133.8, 126.8, 118.7, 112.8, 112.7, 31.2; HRMS (ESI+): *m/z* calcd. for $C_{13}H_9NBr^{81}BrO$ 354.9025 $[M]^+$, found 354.9024.

1.2.6 Synthesis of 3,7-divinyl-*N*-methylphenoxazine (4)

A solution of 3,7-dibromo-*N*-methylphenoxazine (**5**, 50 mg, 0.14 mmol), 4,4,5,5-tetramethyl-2-vinyl-1,3,2-dioxaborolane (0.10 mL, 0.56 mmol) and $Pd(PPh_3)_4$ (16 mg, 14 µmol) in a degassed mixture of THF (1.7 mL) and aqueous NaOH (2.8 M, 0.3 mL) was heated to 80 °C for 24 h. After cooling to room temperature, H_2O (5 mL) and brine (2 mL) were added, and the mixture was extracted with dichloromethane (3 × 20 mL). The combined organic extracts were dried over $MgSO_4$, filtered, and the solvent was removed under reduced pressure. Column chromatography (triethylamine-impregnated silica gel, cyclohexane/ethyl acetate: 15/1) yielded 3,7-divinyl-*N*-methylphenoxazine (**4**, 22 mg, 88 µmol, 63%) as a white solid. R_f 0.54 (cyclohexane/ethyl acetate: 10/1); ^{1}H NMR (500 MHz, $CDCl_3$): δ 6.85 (dd, *J* = 8.2, 2.1 Hz, 2H), 6.82 (d, *J* = 2.1 Hz, 2H), 6.53 (dd, *J* = 17.5, 10.8 Hz, 2H), 6.46 (d, *J* = 8.2 Hz, 2H), 5.55 (dd, *J* = 17.5, 0.8 Hz, 2H), 5.10 (dd, *J* = 10.8, 0.9 Hz, 2H), 3.06 (s, 3H); ^{13}C NMR (125 MHz, $CDCl_3$): δ 145.4, 135.9, 134.2, 131.2, 122.6, 112.4, 111.6, 111.3, 31.2; HRMS (APCI+): *m/z* calcd. for $C_{17}H_{16}NO$ 250.1226 $[M+H]^+$, found 250.1228.

1.2.7 Synthesis of crosslinked poly(3-vinyl-*N*-methylphenoxazine) (X-PVMPO)

A solution of azobisisobutyronitrile (4.0 mg, 24 µmol) in dry and degassed THF (0.3 mL) was added to a stirred solution of 3-vinyl-*N*-methylphenoxazine (**3**, 270 mg, 1.21 mmol) and 3,7-divinyl-*N*-methyl-phenoxazine (**4**, 30 mg, 0.12 mmol) in dry and degassed THF (1.5 mL). The flask was immediately immersed in a pre-heated oil bath, and the solution was stirred at 60 °C for 5 d. The reaction was quenched by adding methanol (2 mL), and the mixture was evaporated to dryness under reduced pressure. The crude product was pestled into a powder, suspended with dichloromethane, allowed to swell until the phase looked homogenious, and precipitated from cyclohexane. The purified crosslinked poly(3-vinyl-*N*-methylphenoxazine) (**X-PVMPO**, 201 mg, 67%) was obtained as an off-white powder. FT-IR (ATR): $\tilde{\nu}_{max}$ = 627 (w), 735 (vs), 801 (m), 848 (w), 1143 (w), 1212 (m), 1272 (vs), 1360 (m), 1430 (w), 1489 (vs), 1598 (w), 2920 (vw) cm^{-1}; elemental analysis: calcd (%) for $C_{15}H_{13}NO$: C 80.69, H 5.87, N 6.27; found: C 80.33, H 6.09, N 6.10; TGA (10 °C min^{-1}, air): onset 423 °C, $T_{d10\%}$ (temperature for 10% weight loss) 420 °C.

Investigation by GC/MS analysis of the monomer ratio in the cyclohexane filtrate after precipitation allowed to estimate the ratio of monomers incorporated in the polymer. The calculated ratio of **3** to **4** in the crosslinked polymer was 7.7 to 1, leading to a higher crosslinkage than the estimated ratio of 10 to 1. So crosslinkage occured statistically at every 8.7th monomeric unit.

1.3 Characterization data

1.3.1 NMR spectra

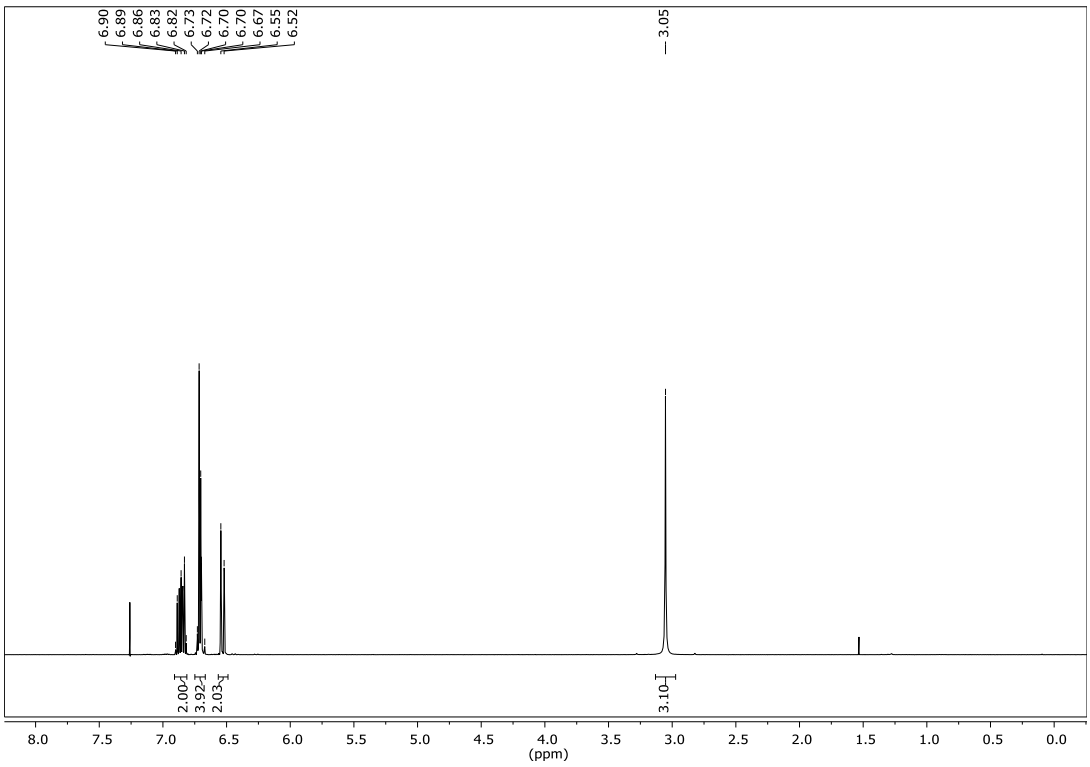

Figure S1. 300 MHz ^{1}H NMR spectrum of *N*-methylphenoxazine (**MPO**) in $CDCl_3$.

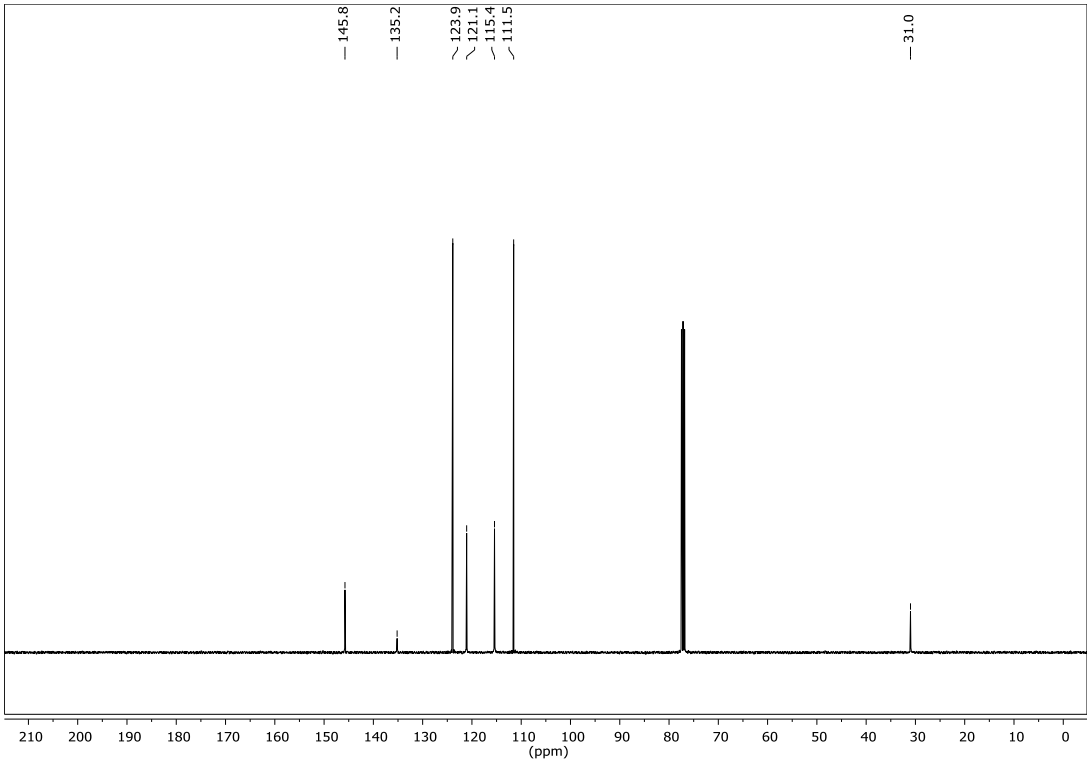

Figure S2. 100 MHz ^{13}C NMR spectrum of *N*-methylphenoxazine (**MPO**) in $CDCl_3$.

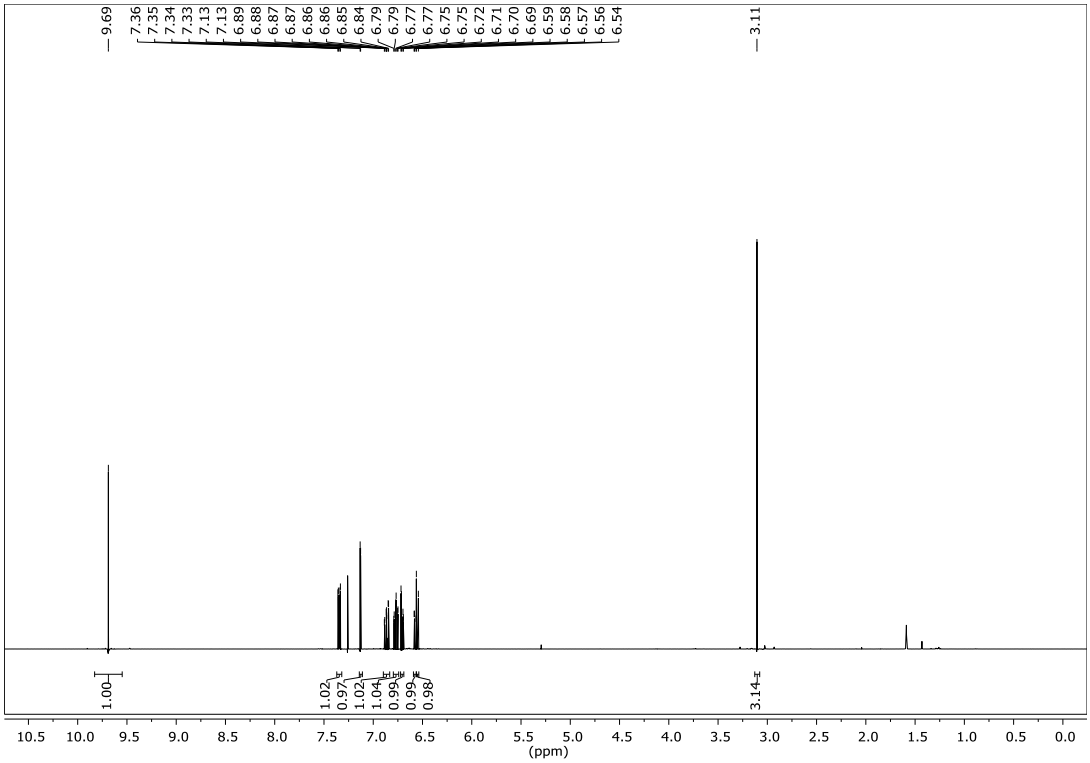

Figure S3. 400 MHz ^{1}H NMR spectrum of *N*-methylphenoxazinyl-3-carbaldehyde (**2**) in $CDCl_3$.

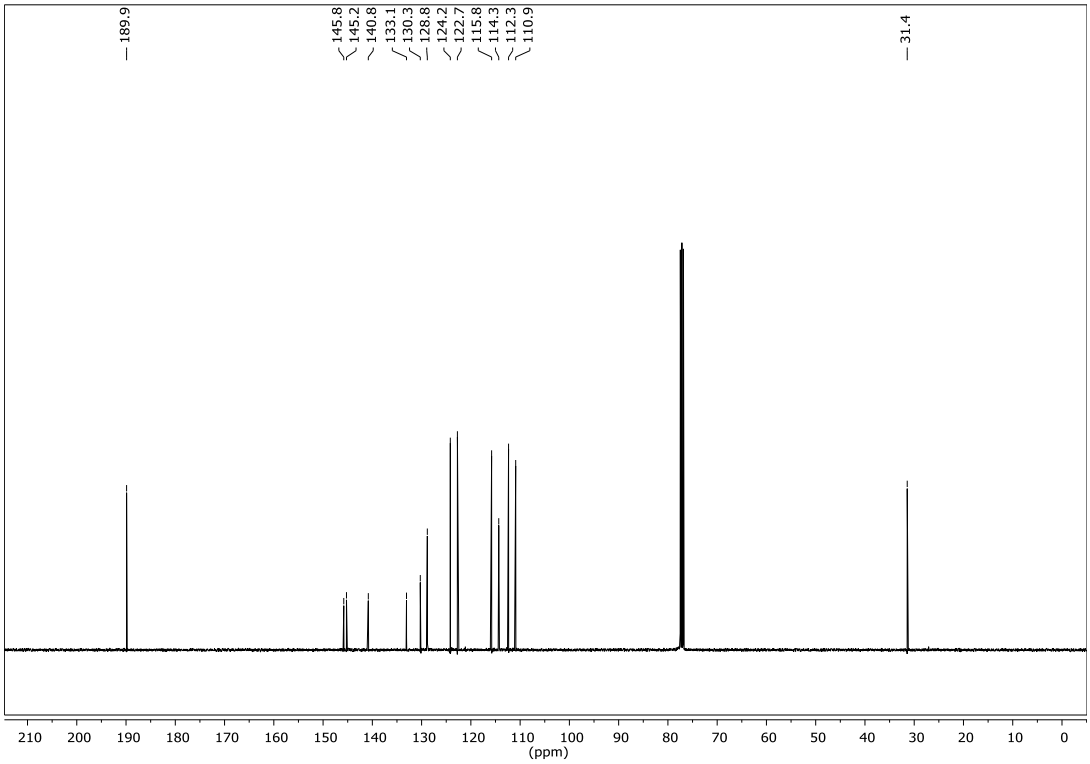

Figure S4. 100 MHz ^{13}C NMR spectrum of *N*-methylphenoxazinyl-3-carbaldehyde (**2**) in $CDCl_3$.

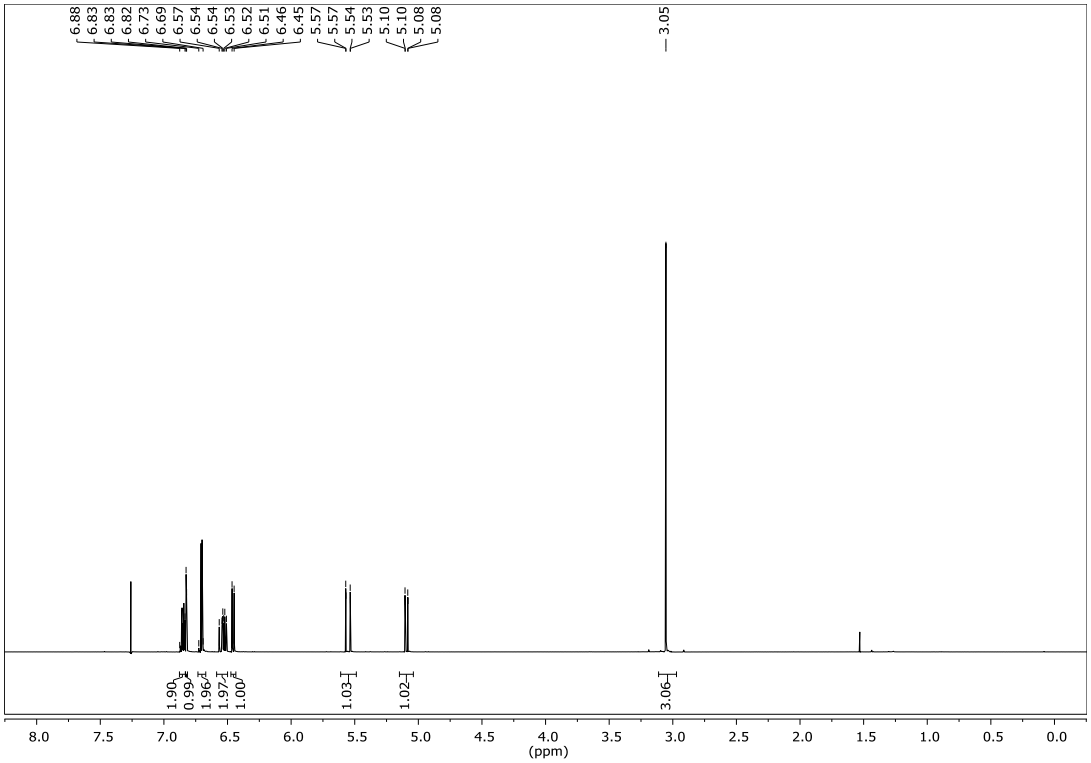

Figure S5. 500 MHz ^{1}H NMR spectrum of 3-vinyl-*N*-methylphenoxazine (**3**) in $CDCl_3$.

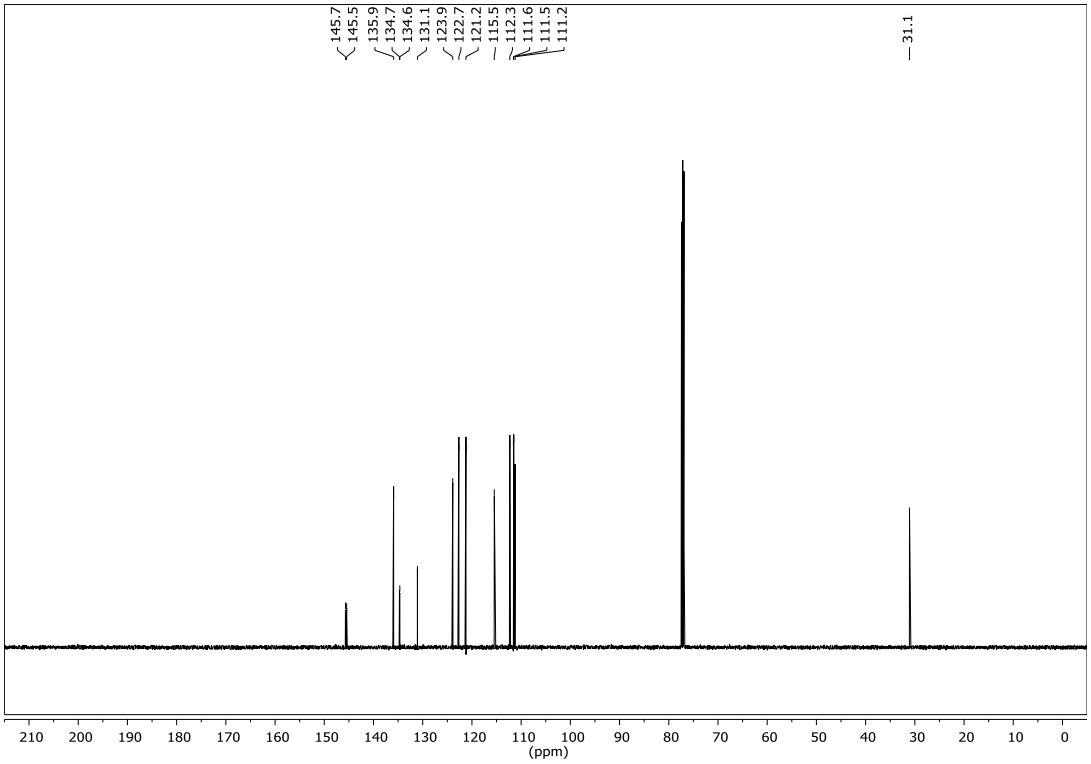

Figure S6. 125 MHz ^{13}C NMR spectrum of 3-vinyl-*N*-methylphenoxazine (**3**) in $CDCl_3$.

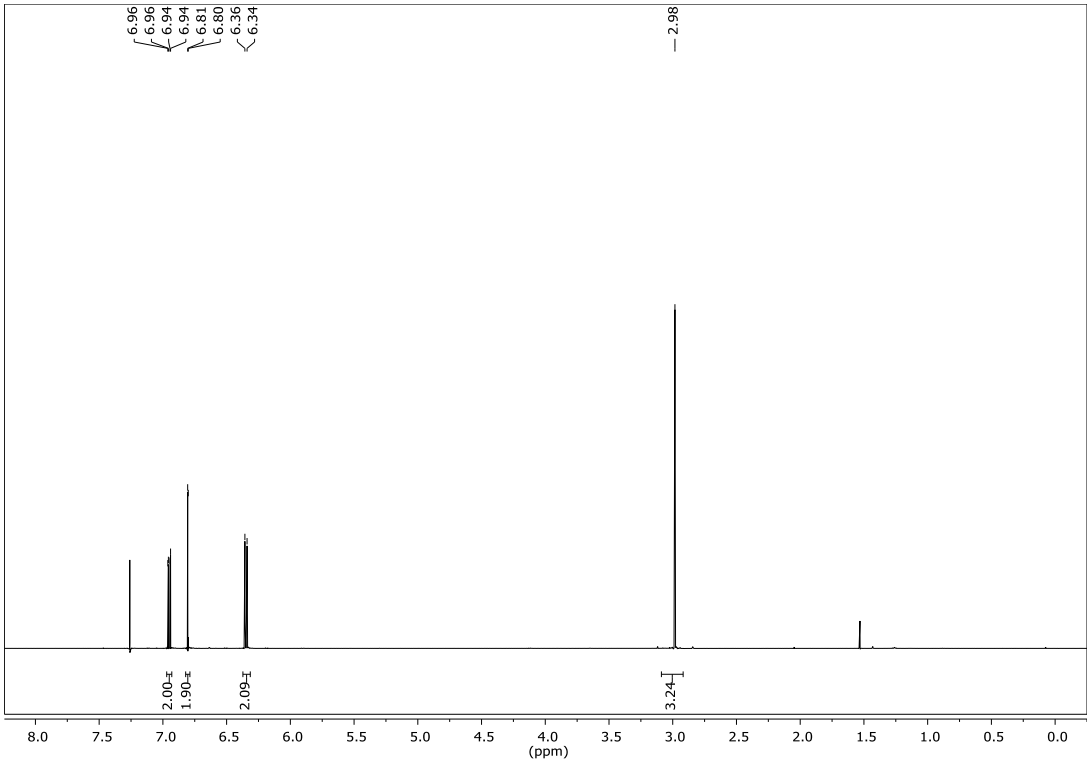

Figure S7. 500 MHz ^{1}H NMR spectrum of 3,7-dibromo-*N*-methylphenoxazine (**5**) in $CDCl_3$.

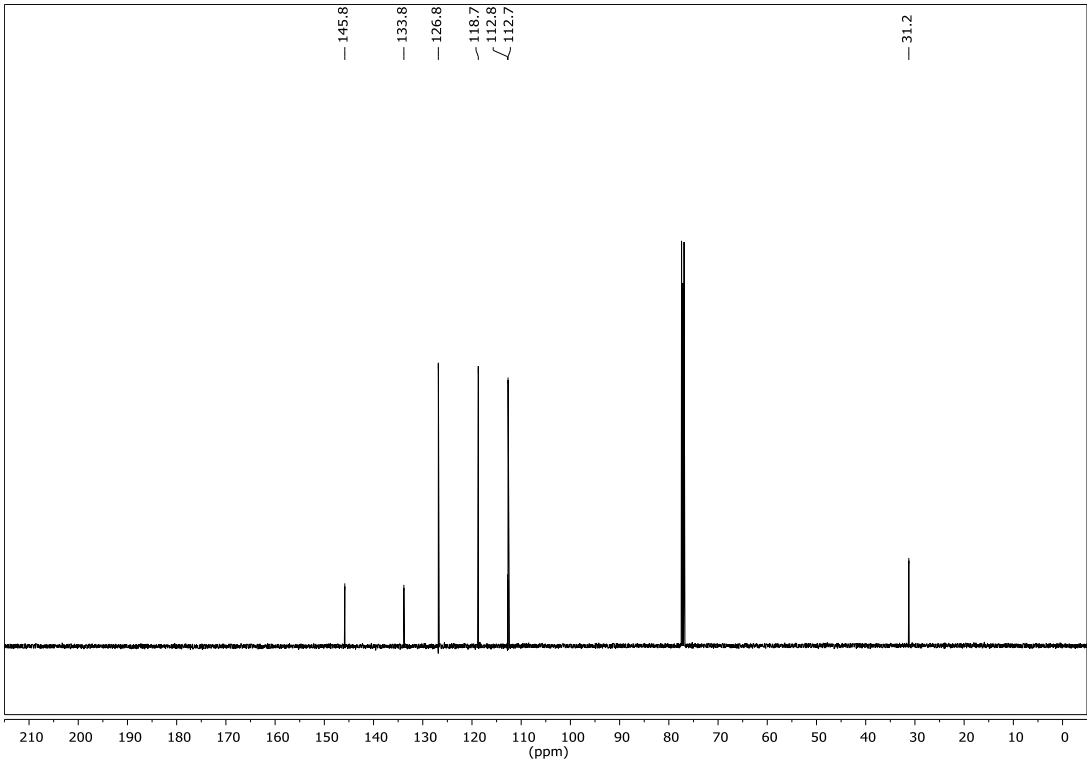

Figure S8. 125 MHz ^{13}C NMR spectrum of 3,7-dibromo-*N*-methylphenoxazine (**5**) in $CDCl_3$.

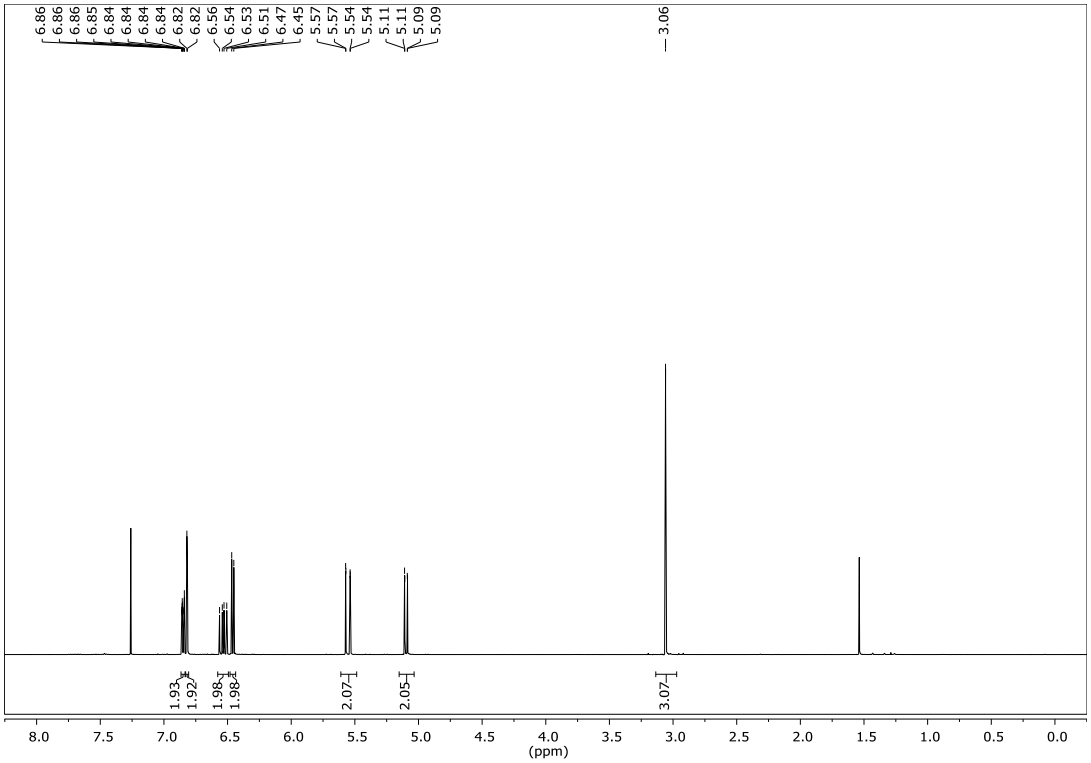

Figure S9. 500 MHz ^{1}H NMR spectrum of 3,7-divinyl-*N*-methylphenoxazine (**4**) in $CDCl_3$.

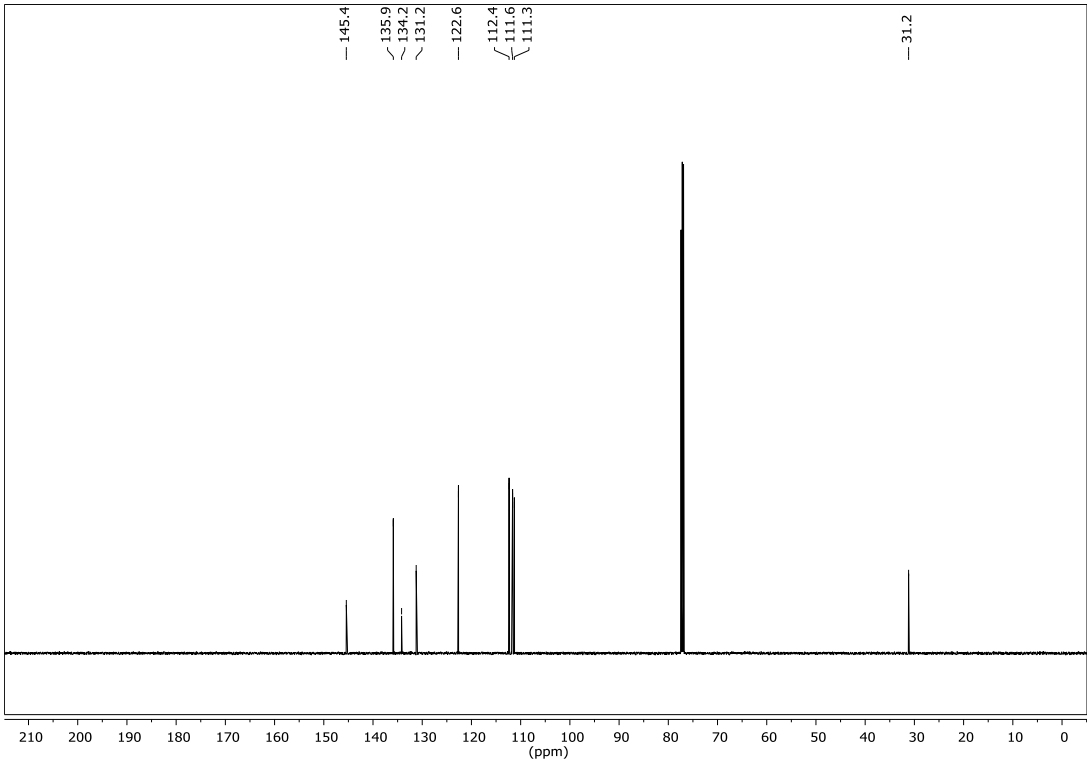

Figure S10. 125 MHz ^{13}C NMR spectrum of 3,7-divinyl-*N*-methylphenoxazine (**4**) in $CDCl_3$.

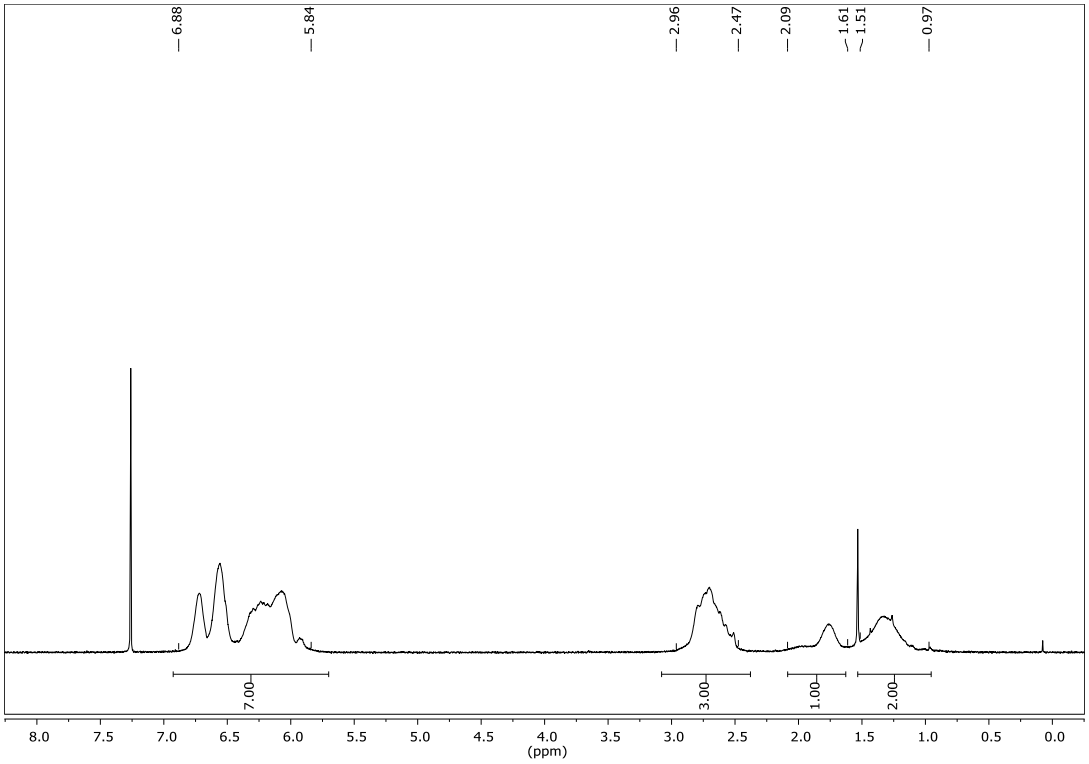

Figure S11. 300 MHz ^{1}H NMR spectrum of poly(3-vinyl-*N*-methylphenoxazine) (**PVMPO**) in $CDCl_3$.

1.3.2 FTIR spectra of PVMPO and X-PVMPO

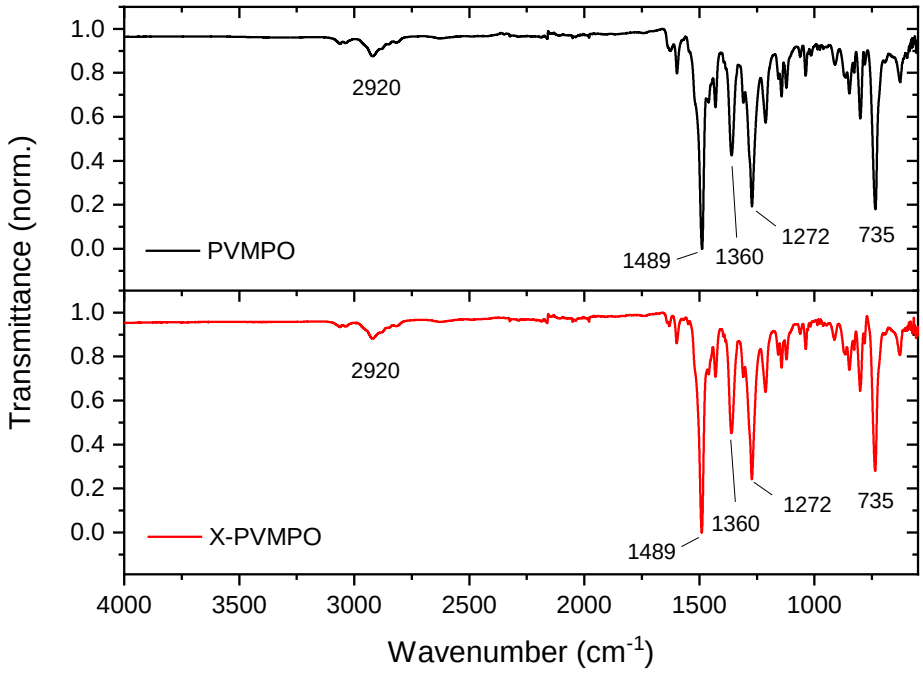

Figure S12. ATR FT-IR spectrum (diamond, 64 scans, res. 2 cm^{-1}) of **PVMPO** (top, black curve) and **X-PVMPO** (bottom, red curve).

1.3.3 Thermal gravimetric analyses (TGA) of PVMPO and X-PVMPO

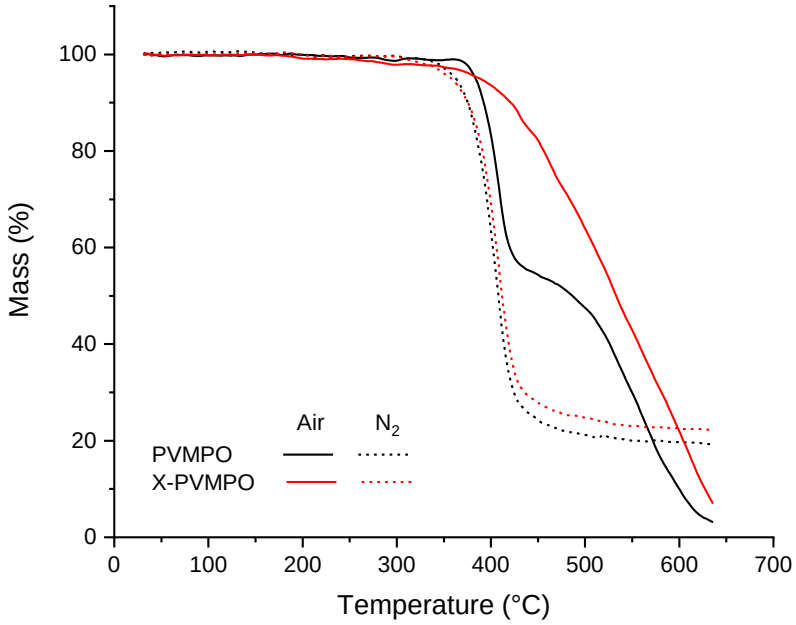

Figure S13. TGA curves of **PVMPO** and **X-PVMPO** in ambient air atmosphere and N_2 at a heating rate of 10 °C min^{-1}.

1.3.4 Differential scanning calorimetry (DSC) measurements of PVMPO and X-PVMPO

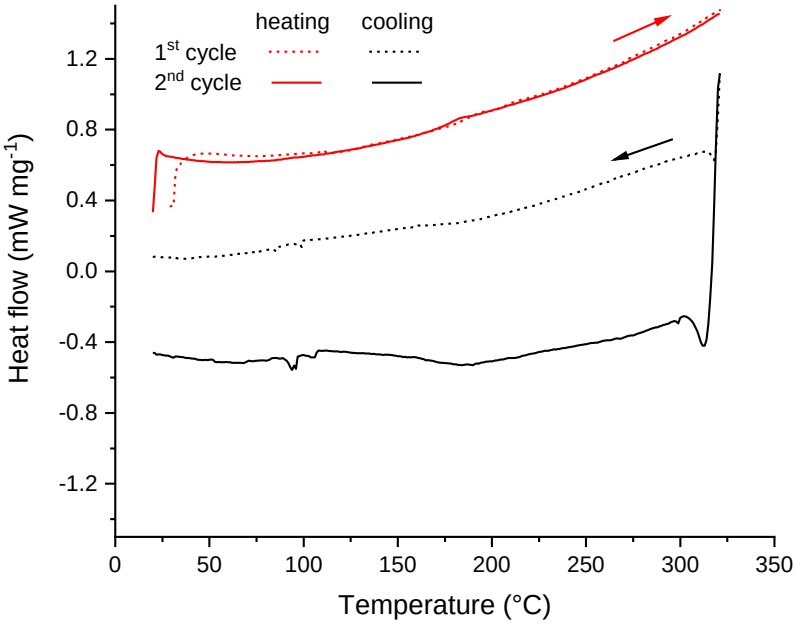

Figure S14. DSC measurement of **PVMPO** in ambient air atmosphere at a heating rate of 10 °C min^{-1}.

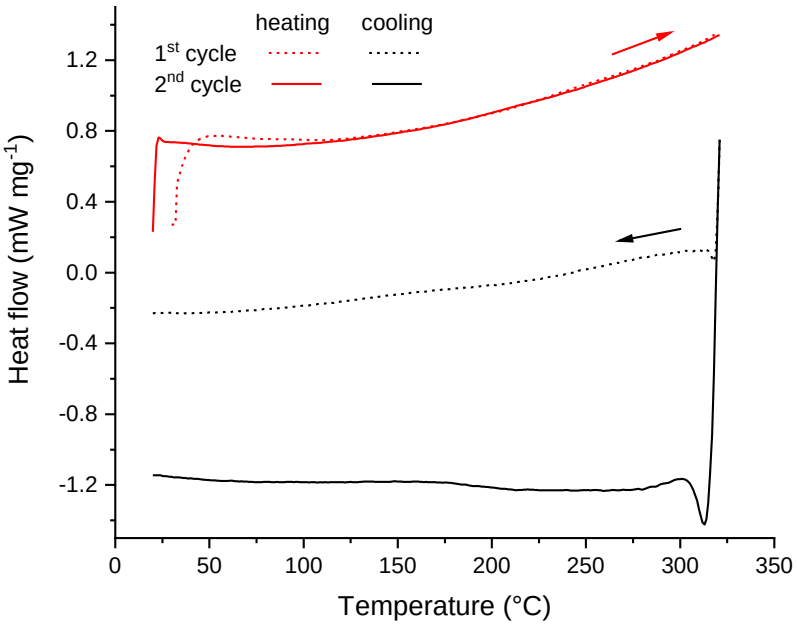

Figure S15. DSC measurement of **X-PVMPO** in ambient air atmosphere at a heating rate of 10 °C min^{-1}.

2 Electrochemical investigations in solution

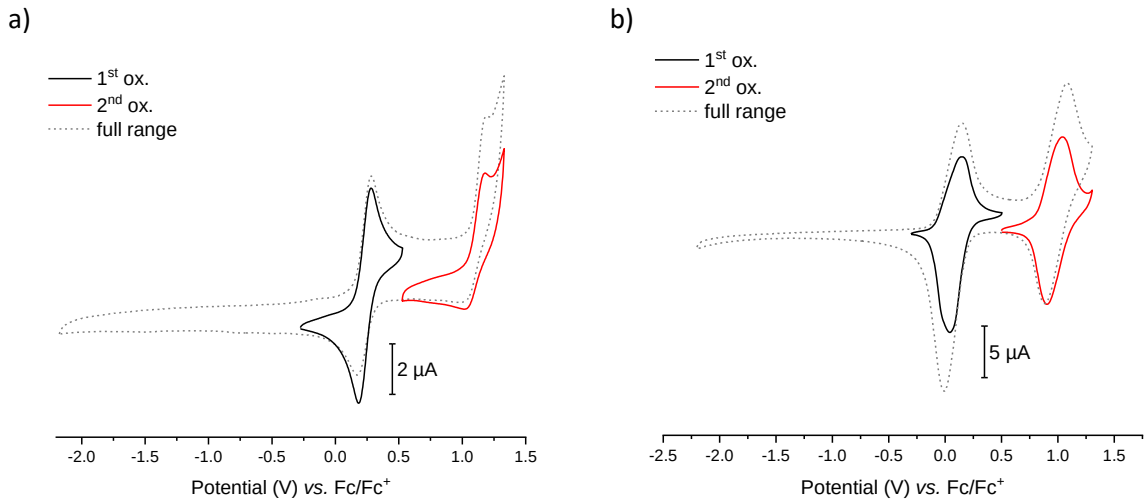

Figure S16. Cyclic voltammograms of a) **MPO** and b) **PVMPO**. Measurements performed in CH_2Cl_2, 1 mM (referred to the redox active group) with 0.1 M *n*-Bu_4NPF_6, at a scan rate of 100 mV s^{-1}; WE: GC, CE: Pt, RE: $Ag/AgNO_3$ (referenced to internal standard Fc/Fc^+).

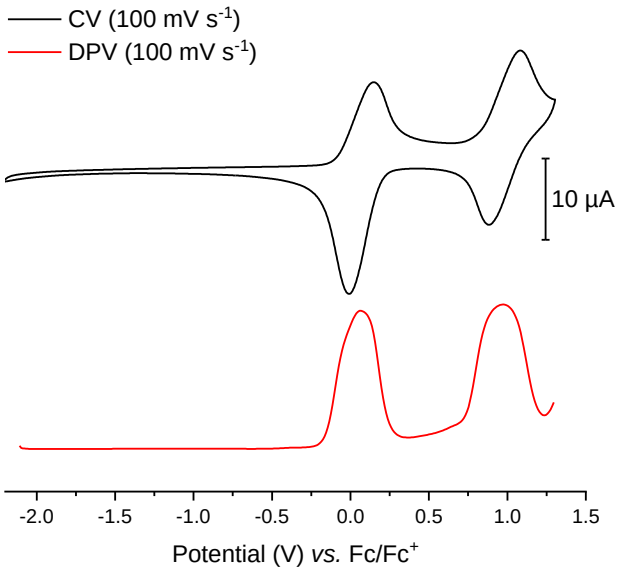

Figure S17. Cyclic voltammogram (CV, top, black curve) and differential pulse voltammogram (DPV, bottom, red curve) of **PVMPO**. Measurements performed in CH_2Cl_2, 1 mM (referred to the redox active group) with 0.1 M *n*-Bu_4NPF_6, at a scan rate of 100 mV s^{-1}; WE: GC, CE: Pt, RE: $Ag/AgNO_3$ (referenced to internal standard Fc/Fc^+).

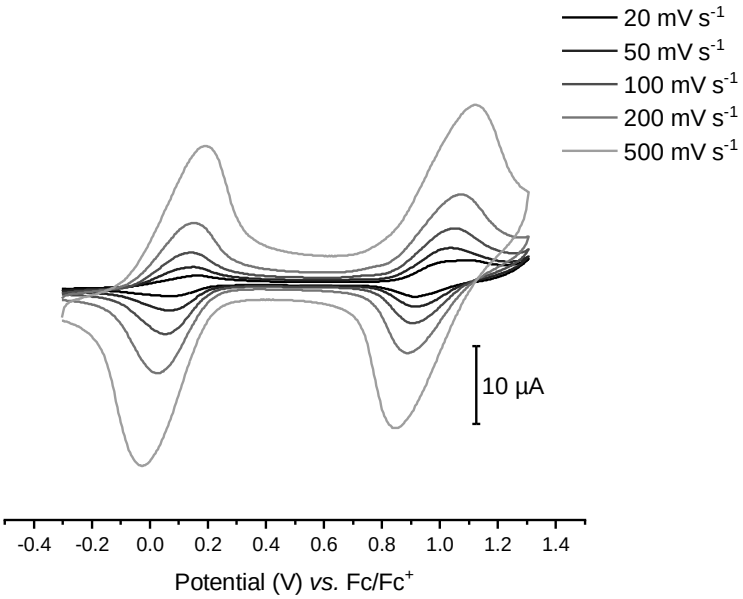

Figure S18. Cyclic voltammograms of **PVMPO** at different scan rates. Measurements performed in CH_2Cl_2, 1 mM (referred to the redox active group) with 0.1 M *n*-Bu_4NPF_6; WE: GC, CE: Pt, RE: $Ag/AgNO_3$ (referenced to internal standard Fc/Fc^+).

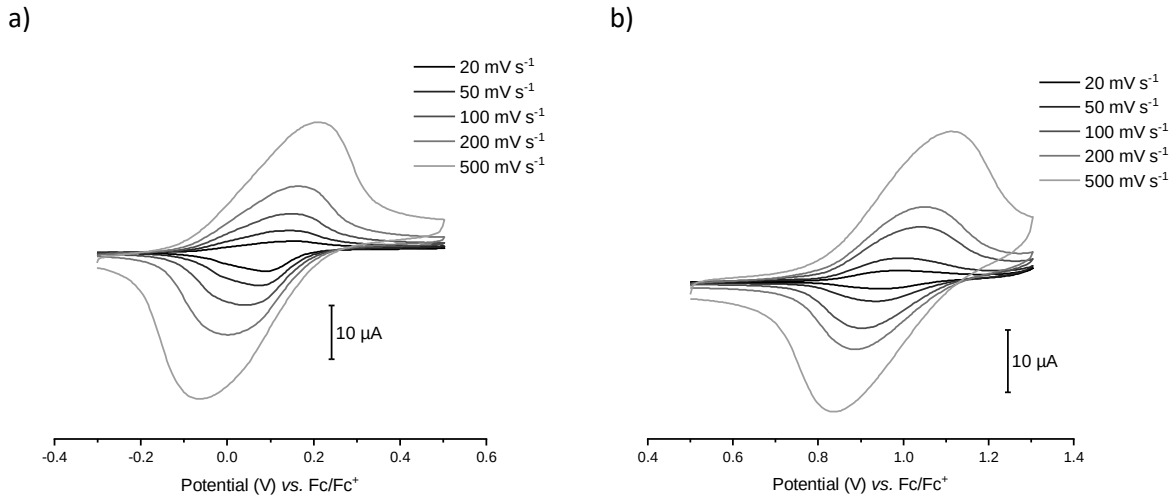

Figure S19. Cyclic voltammograms of **PVMPO** at different scan rates: a) 1st redox reaction and b) 2nd redox reaction. Measurements performed in CH_2Cl_2, 1 mM (referred to the redox active group) with 0.1 M *n*-Bu_4NPF_6; WE: GC, CE: Pt, RE: $Ag/AgNO_3$ (referenced to internal standard Fc/Fc^+).

3 Investigations on (X-)PVMPO-based composite electrodes

All composite electrodes were fabricated as described in the Experimental Procedures section of the manuscript.

3.1 SEM/EDS measurements

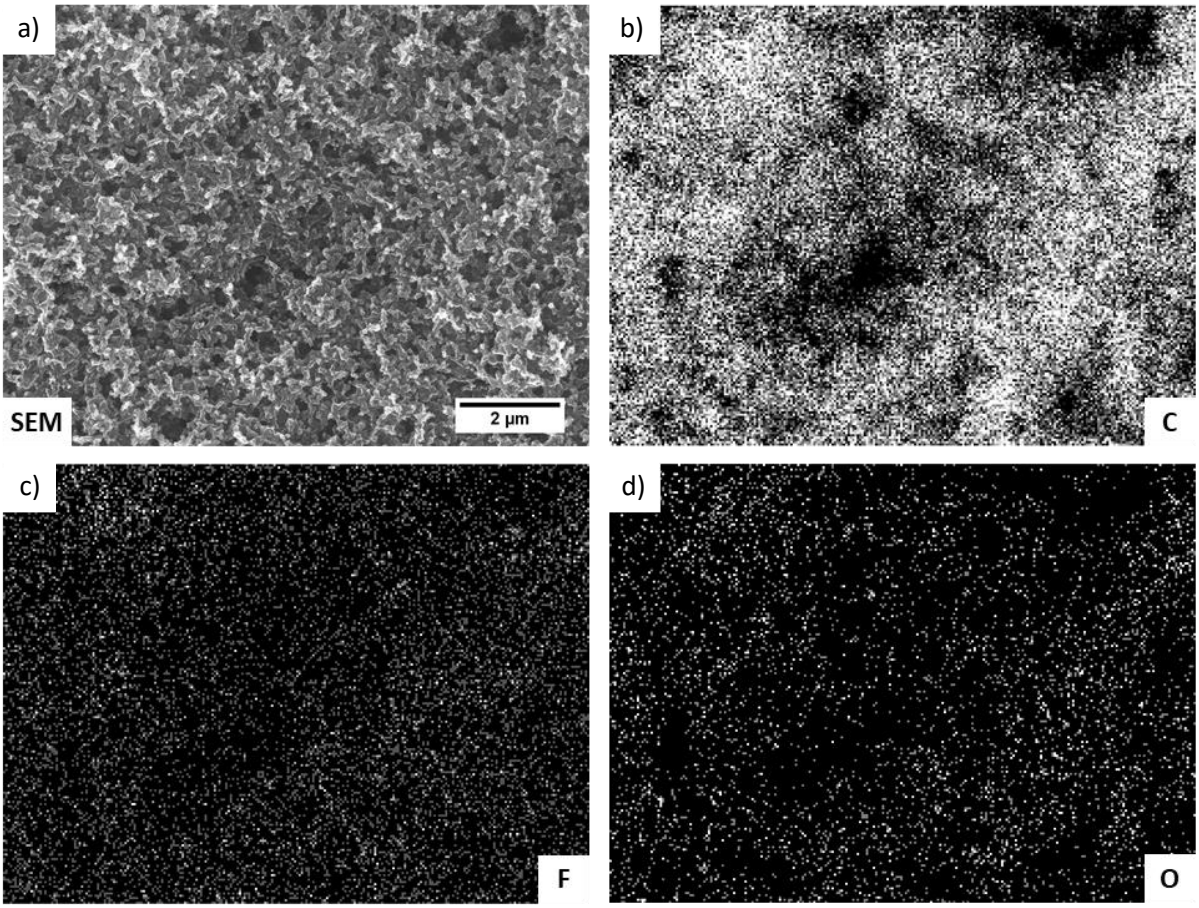

Figure S20. a) SEM micrograph (10,000x magnification) and EDS mappings of b) carbon, c) fluorine, and d) oxygen of a pristine **PVMPO**-based electrode.

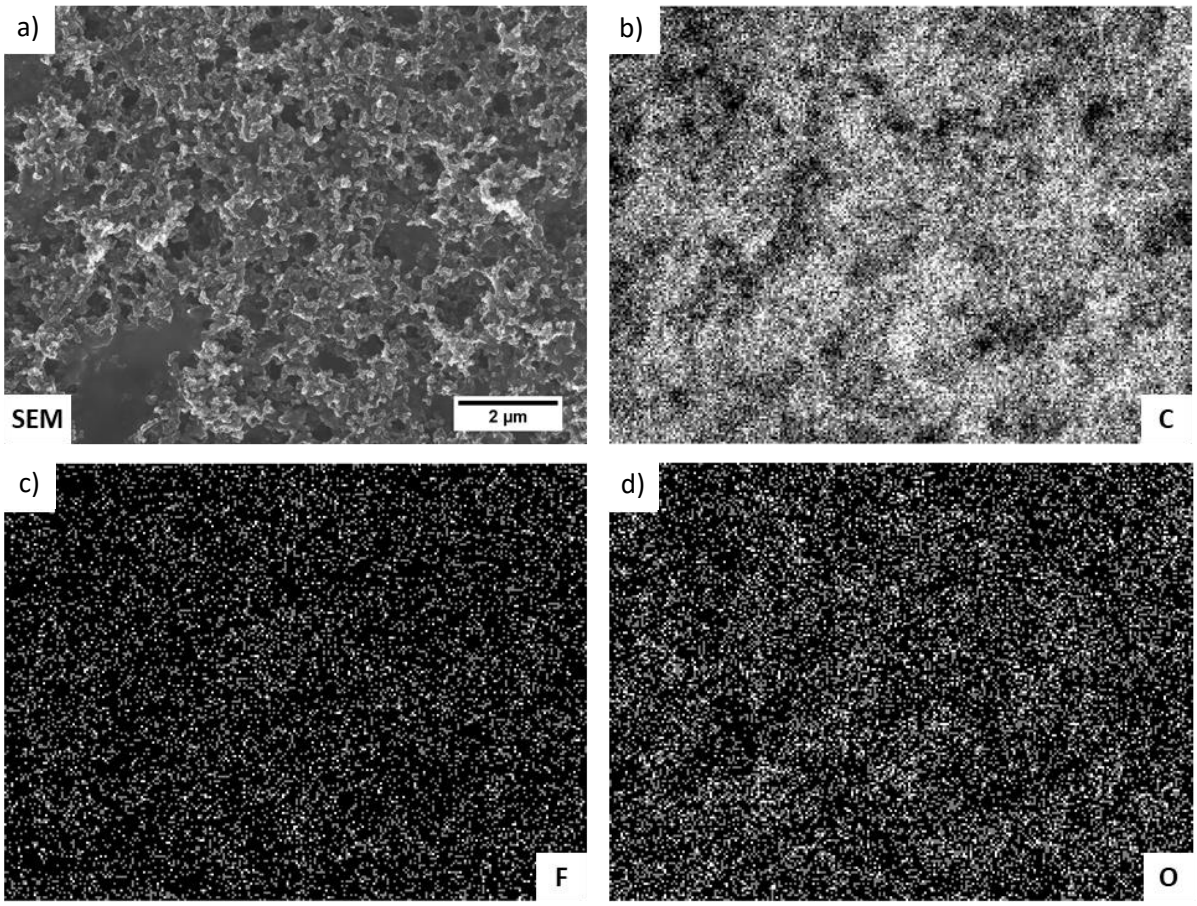

Figure S21. a) SEM micrograph (10,000x magnification) and EDS mappings of b) carbon, c) fluorine, and d) oxygen of a pristine **X-PVMPO**-based electrode.

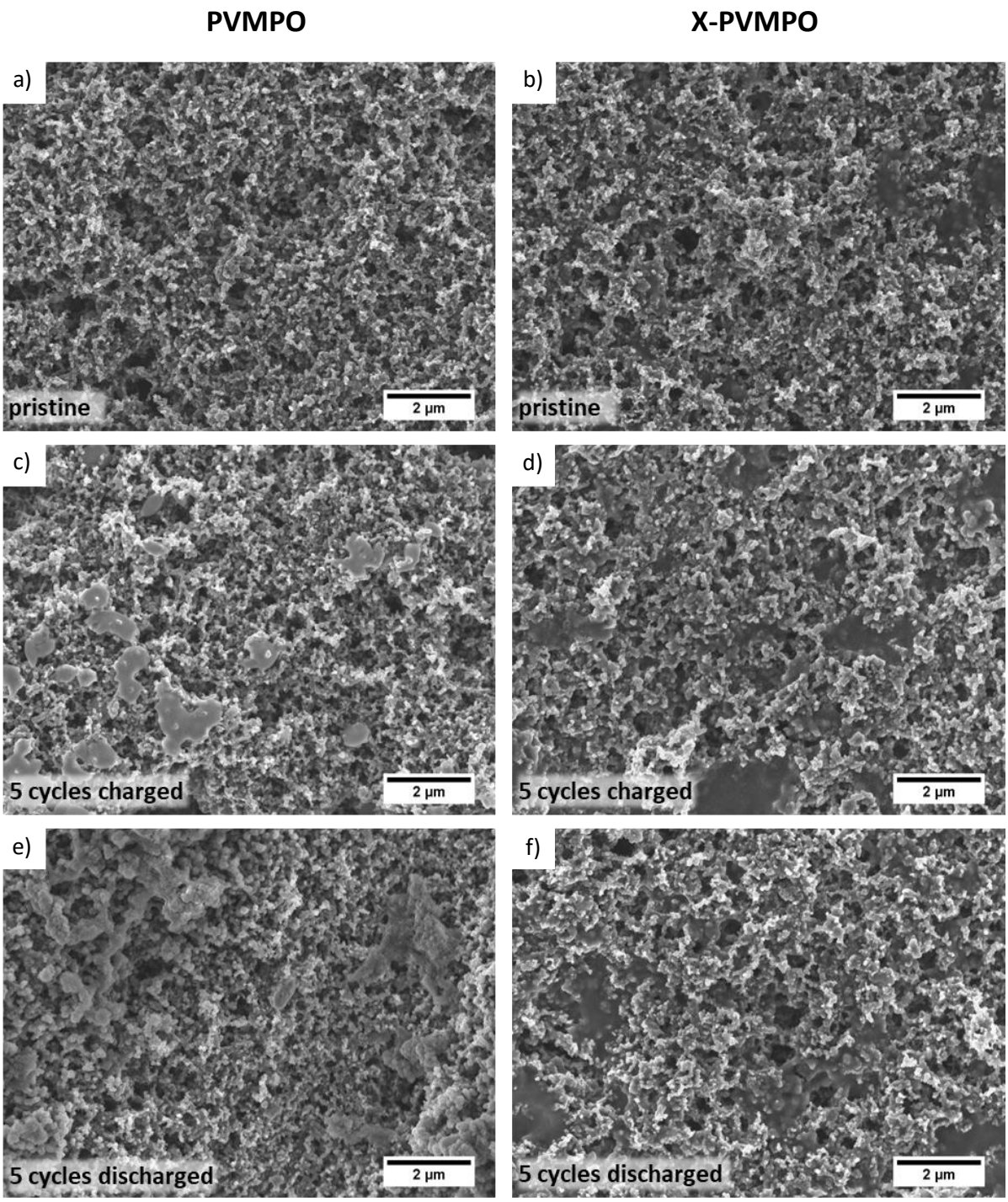

Figure S22. SEM micrographs (10,000x magnification) in cross-section view of **PVMPO**- (a, c, e) and **X-PVMPO**-based (b, d, f) electrodes: pristine (a, b), after 5 cycles in the charged (c, d), and in the discharged (e, f) state.

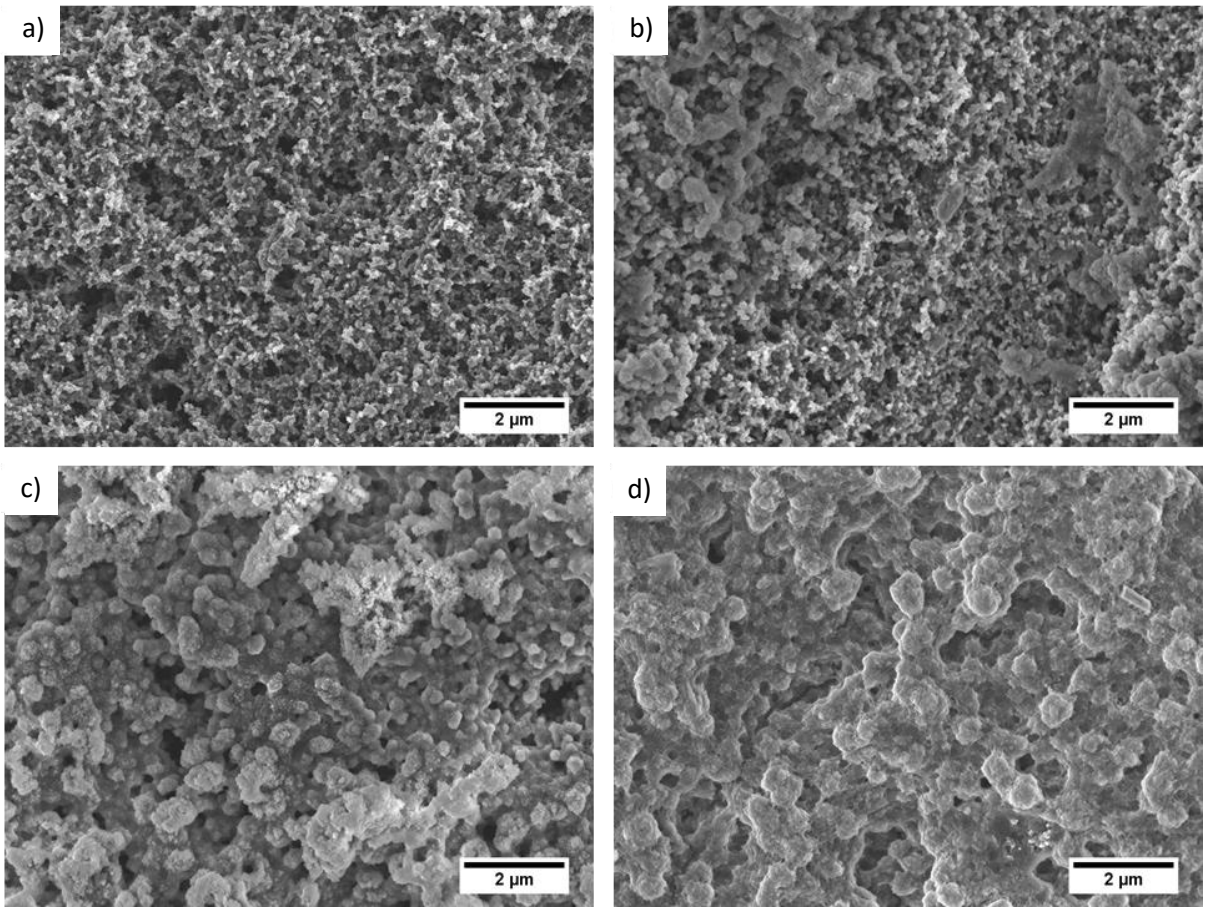

Figure S23. SEM micrographs (10,000x magnification) in cross-section view of **PVMPO**-based electrodes: a) pristine, b) after 5 cycles, c) after 50 cycles, and d) after 1000 cycles in discharged state.

3.2 Cyclic voltammetry investigations

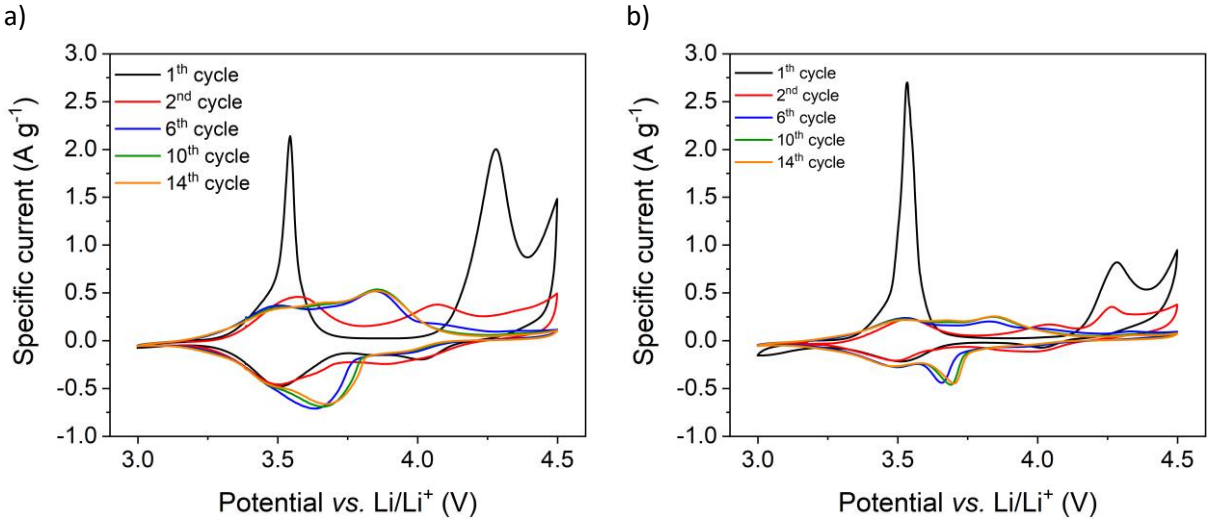

Figure S24. Cyclic voltammograms of a) a **PVMPO** and b) a **X-PVMPO**-based composite electrode (0.16 mg cm^{-2}) between 3 and 4.5 V *vs.* Li/Li$^+$ measured at a scan rate of 0.5 mV s^{-1}.

4 Spectroscopic investigations

4.1 UV/Vis/NIR spectroscopy

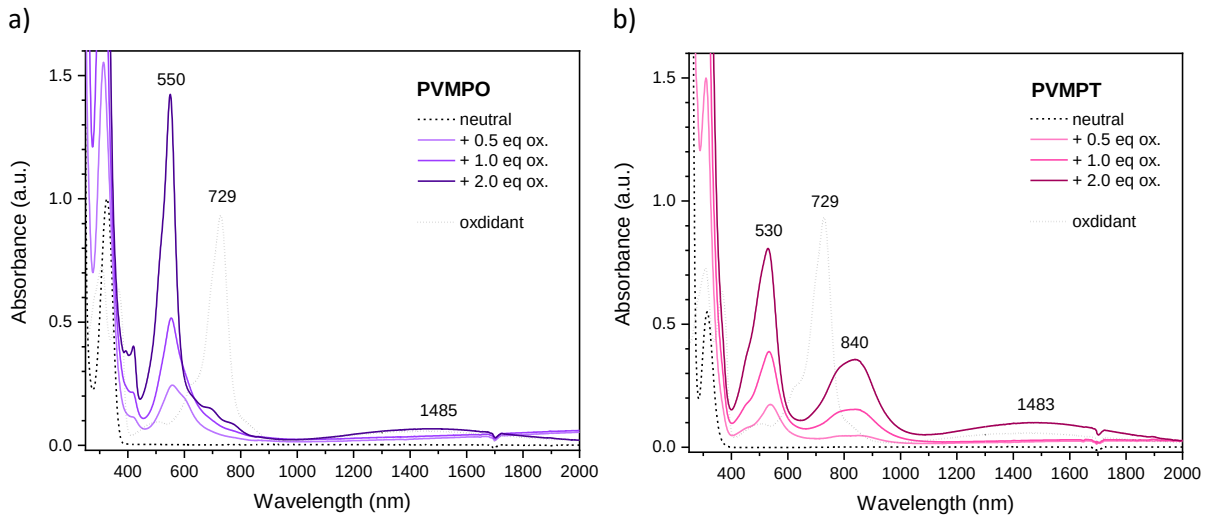

Figure S25. UV/Vis/NIR spectra of a) **PVMPO** and b) **PVMPT** in its neutral states and after the addition of 0.5, 1.0 and 2.0 equivalents of the oxidant tris-(4-bromophenyl)-ammoniumyl hexachloroantimonate in CH_2Cl_2 (0.1 mM referred to the redox active group).

4.2 Spectroelectrochemical measurements

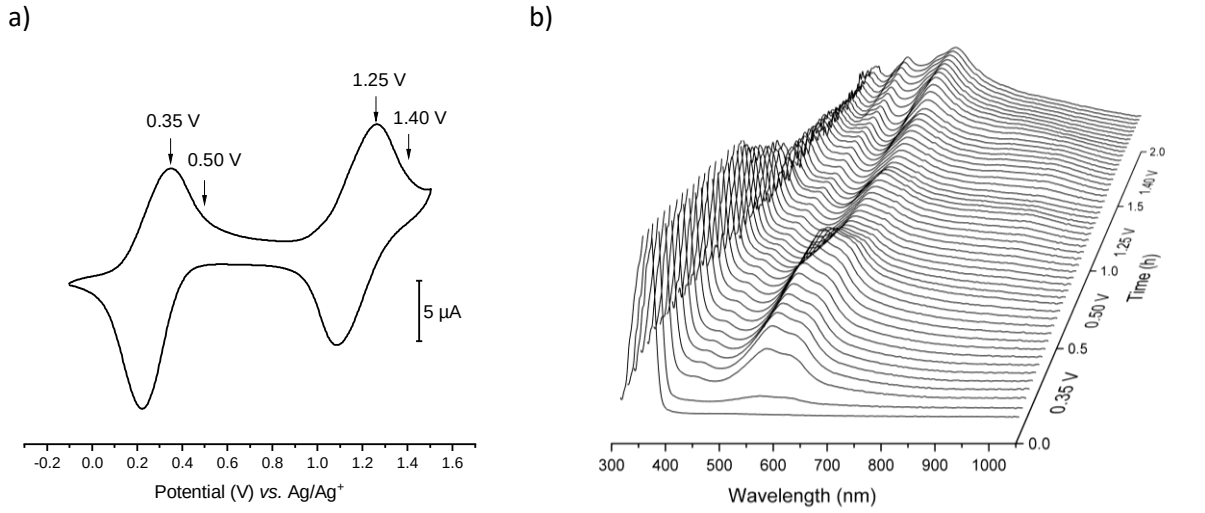

Figure S26. a) Cyclic voltammogram of **PVMPO** in CH_2Cl_2, 1 mM (referred to the redox active group) with 0.1 M *n*-Bu_4NPF_6 at a scan rate of 100 mV s^{-1} (WE: GC, CE: Pt, RE: $Ag/AgNO_3$), and b) spectroelectrochemical measurements of **PVMPO**: UV/Vis spectra recorded during chronoamperometric experiment in CH_2Cl_2, 10 mM (referred to the redox active group) with 0.2 M *n*-Bu_4NPF_6, applied for various potentials *vs.* Ag/Ag^+ (WE: Pt net, CE: Pt, RE: $Ag/AgNO_3$).

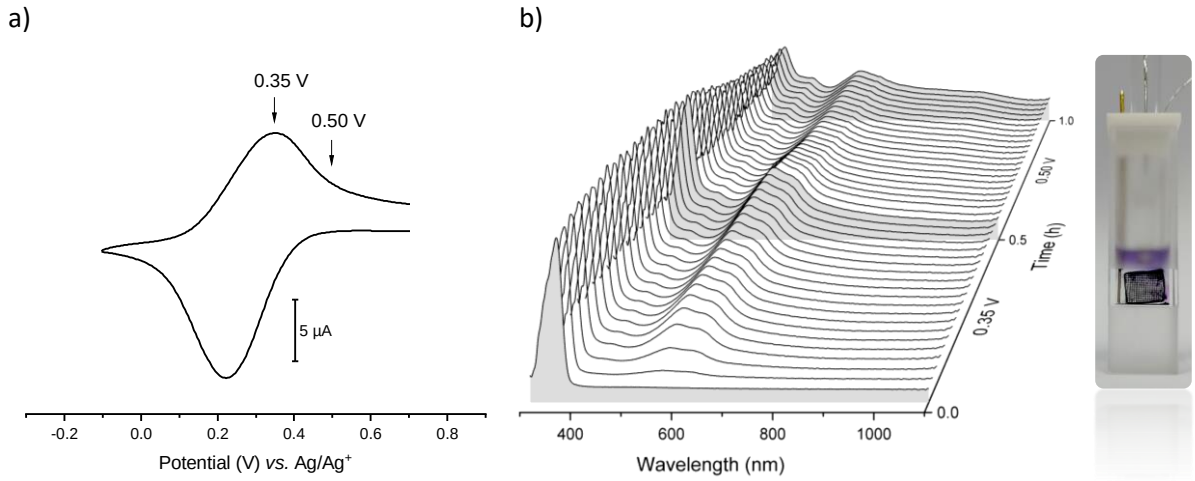

Figure S27. a) Cyclic voltammogram of **PVMPO** in CH_2Cl_2, 1 mM (referred to the redox active group) with 0.1 M *n*-Bu_4NPF_6 at a scan rate of 100 mV s^{-1} (WE: GC, CE: Pt, RE: $Ag/AgNO_3$), and b) spectroelectrochemical measurements of **PVMPO**: UV/Vis spectra recorded during chronoamperometric experiment in CH_2Cl_2, 10 mM (referred to the redox active group) with 0.2 M *n*-Bu_4NPF_6, applied for various potentials versus Ag/Ag^+ (WE: Pt net, CE: Pt, RE: $Ag/AgNO_3$).

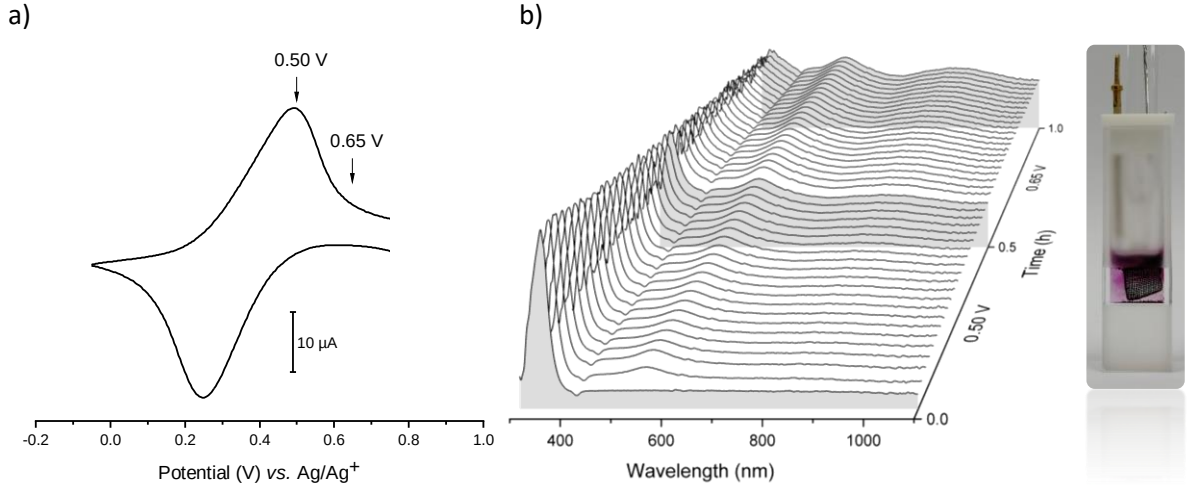

Figure S28. a) Cyclic voltammogram of **PVMPT** in CH_2Cl_2, 1 mM (referred to the redox active group) with 0.1 M *n*-Bu_4NPF_6 at a scan rate of 100 mV s^{-1} (WE: GC, CE: Pt, RE: $Ag/AgNO_3$), and b) spectroelectrochemical measurements of **PVMPT**: UV/Vis spectra recorded during chronoamperometric experiment in CH_2Cl_2, 10 mM (referred to the redox active group) with 0.2 M *n*-Bu_4NPF_6, applied for various potentials versus Ag/Ag^+ (WE: Pt net, CE: Pt, RE: $Ag/AgNO_3$).

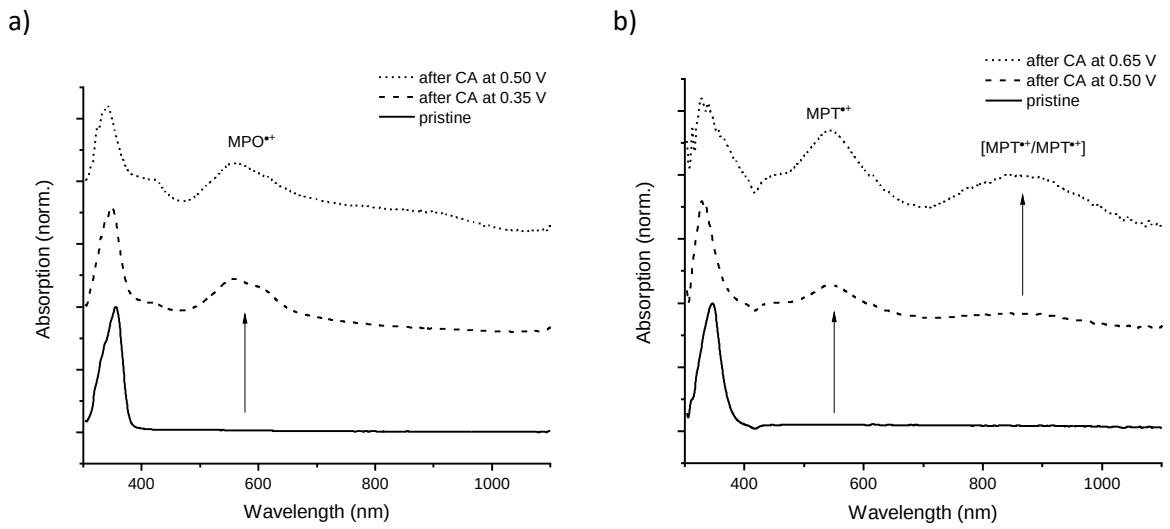

Figure S29. UV/Vis spectra of a) **PVMPO** and b) **PVMPT** recorded during chronoamperometric experiments in CH_2Cl_2, 10 mM (referred to the redox active group) with 0.2 M *n*-Bu_4NPF_6, applied versus Ag/Ag^+ (WE: Pt net, CE: Pt, RE: $Ag/AgNO_3$). The spectra shown were recorded before applying the chronoamperometric experiment (pristine, solid curve) and after the indicated potential steps (dashed curves). Each step was held for 0.5 h.

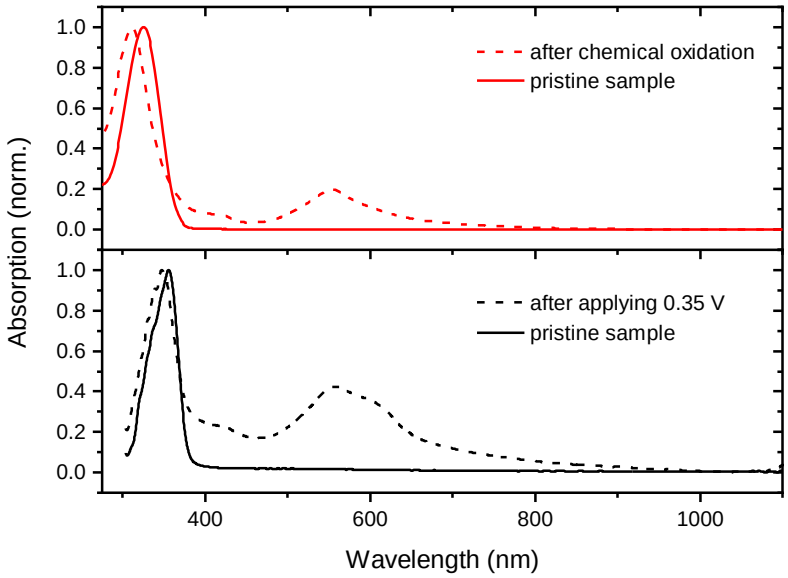

Figure S30. Comparison of UV/Vis spectra of **PVMPO** in its neutral state (pristine, solid curves) and oxidized state (dashed curves) after chemical oxidation (red curves, top) and after chronoamperometric experiment at a potential of 0.35 V versus Ag/Ag^+ (black curves, bottom). Chemical oxidation was performed by the addition of 1.0 equivalent of the oxidant tris-(4-bromophenyl)-ammoniumyl hexachloroantimonate in CH_2Cl_2, 0.1 mM (referred to the redox active group). The chronoamperometric experiment was performed in CH_2Cl_2, 10 mM (referred to the redox active group) with 0.2 M *n*-Bu_4NPF_6, the indicated potential was applied for a duration of 0.5 h (WE: Pt net, CE: Pt, RE: $Ag/AgNO_3$).

5 DFT calculations on model compound 6

DFT calculations were performed with the TURBOMOLE v7.3 program package.[1] The resolution-of-identity[2] (RI, RIJDX for SP) approximation for the Coulomb integrals was used in all DFT calculations employing matching auxiliary basis set def2-XVP/J.[3] Further, the D3 dispersion correction scheme[4,5] with the Becke-Johnson damping function was applied.[6,7] The geometries of all molecules were first optimized without symmetry restrictions (in oxidation state ***A***) with the PBEh-3c[8] composite scheme followed by harmonic vibrational frequency analysis to confirm minima as stationary points. This geometry was used as an input for further geometry optimizations in oxidations states ***A*** to ***C***. They were each optimized on the B3LYP[9,10]-D3/def2-TZVP level of theory. Structures were optimized with unrestricted orbitals for the oxidation state ***B*** and with restricted orbitals for the oxidation states ***A*** and ***C***. For vibrational contributions and the free energy calculations the rigid-rotor-harmonic-oscillator approximation was made.

6 was chosen as model compound for **PVMPO**, containing two subunits (see Figure 5C, Manuscript). It can exist in the three oxidation states ***A*** (neutral), the ***B*** (half-oxidized), and ***C*** (fully oxidized).

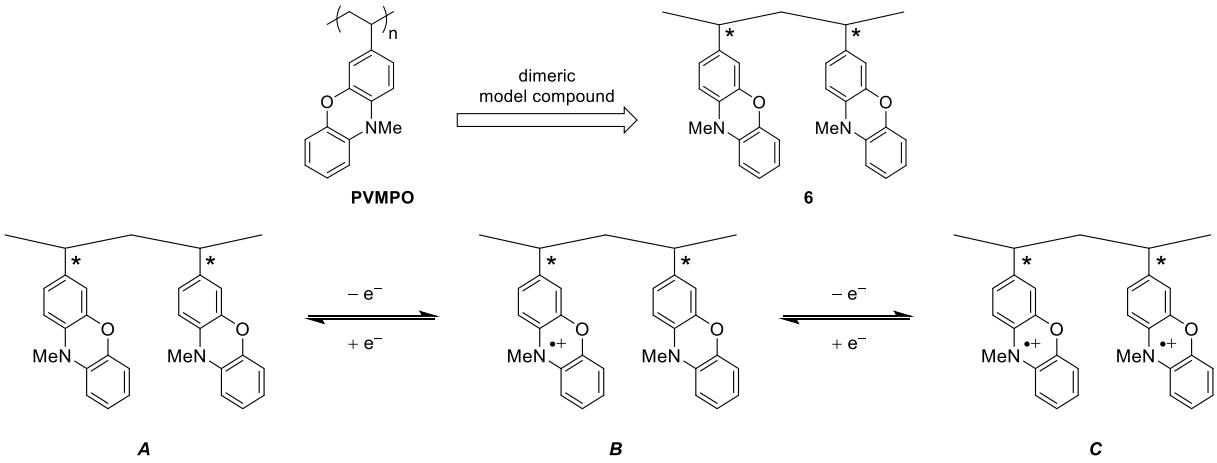

There are four constitutional and confirmational isomers of model compound **6**: **6a**–**6d**. Calculations were performed for all four isomers.

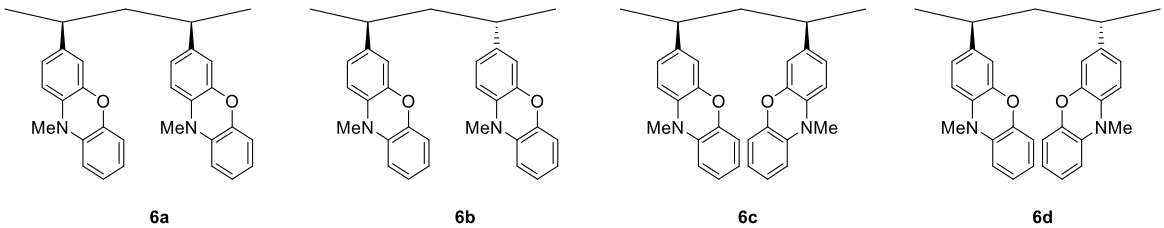

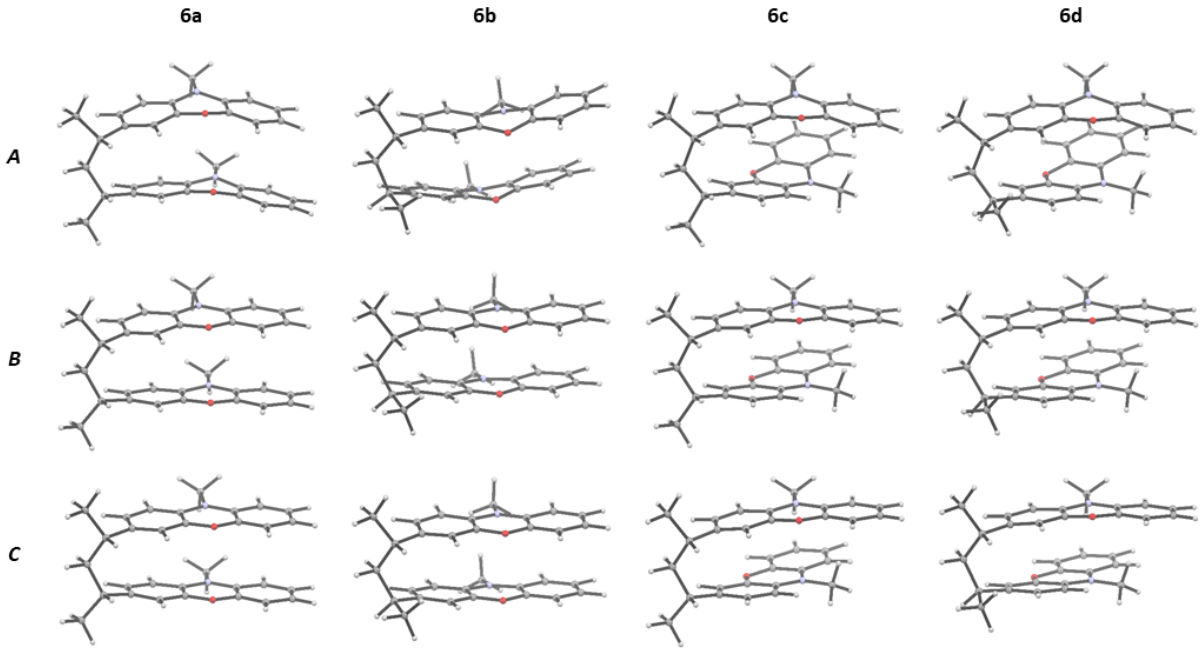

Figure S31. Optimized structures of isomers **6a–d** in oxidation state ***A***, ***B***, and ***C*** (B3LYP-D3/def2-TZVP+COSMO).

Table S1. Calculated geometrical parameters (B3LYP-D3/def2-TZVP+COSMO) for model compounds **6a–d**, *N*-methylphenoxazine (**MPO**), and *N*-methylphenothiazine (**MPT**).

		$d_{NO\text{-}Centroid}$ (Å)	θ (°) [a]
6a	***A***	3.745	158.8
	B	3.468	174.1
	C	3.330	177.8
6b	***A***	3.830	159.9
	B	3.466	175.0
	C	3.323	178.0
6c	***A***	4.142	161.5
	B	3.981	170.4
	C	4.141	173.8
6d	***A***	4.160	161.6
	B	4.010	170.2
	C	4.206	173.5
MPO	***A***	-	155.5
	B	-	175.1
	C	-	178.3
MPT	***A***	-	139.2
	B	-	165.4
	C	-	174.0

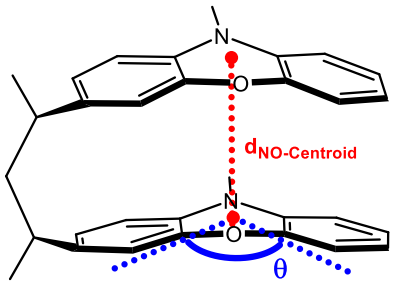

[a] For **6a–d** average of both **MPO** units.

Table S2. Energies obtained for all structures after geometry optimization and calculation of the harmonic vibrational frequencies (PBEh3c/def2-mSVP) and electronic energies after the optimization on the B3LYP-D3/def2-TZVP level of theory.

	A			***B***	***C***
	E (E_h) [a]	ZPE (E_h) [a]	*E* (E_h) [b]	*E* (E_h) [b]	*E* (E_h) [b]
6a	−1456.1659854	0.5573309	−1459.1324673	−1458.9686602	−1458.7813096
6b	−1456.1649007	0.5575544	−1459.1310541	−1458.9671235	−1458.7800112
6c	−1456.1687895	0.5572427	−1459.1353189	−1458.9671734	−1458.7734675
6d	−1456.1663279	0.5576664	−1459.1326187	−1458.9648105	−1458.7717174
MPO	−630.5980451	0.2156941	−631.896336	−631.720851	−631.5005811
MPT	−953.2981099	0.2132727	−954.845195	−954.665759	−954.4501925

[a] PBEh3c/def2-mSVP.

[b] B3LYP-D3/def2-TZVP.

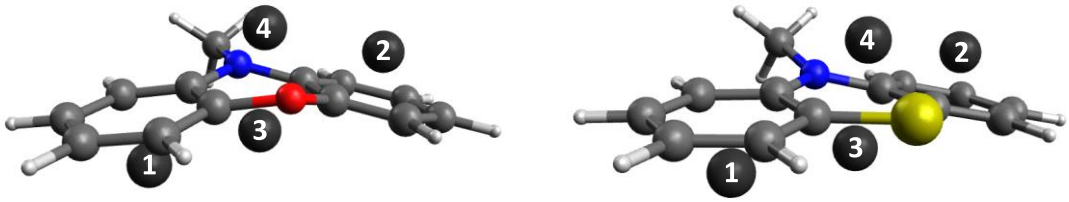

Figure S32. Representative positions of the dummy atoms for the $NICS_1$(iso) calculations (left: **MPO**, right: **MPT**). Each dummy atom is positioned 1 Å above the respective ring plane. Dummy atoms 1 and 3 are on the convex side, 2 and 4 are on the concave side of the molecule.

Nucleus independent chemical shift (NICS)[11,12] values were calculated using the Gaussian 16 program package[13] applying the standard Gauge-Including Atomic Orbitals (*GIAO*) method on the B3LYP/6-31G* level of theory. Negative NICS values indicate a diatropic ring current (associated with an aromatic character), while positive NICS values indicate a paratropic ring current (associated with an antiaromatic character). In the neutral state for both (**MPO** and **MPT**) the NICS values of the peripheric benzene rings indicate high aromaticity and the NICS value of the heteroaromatic rings indicate a slightly antiaromatic character (except for the concave position of **MPT** with a slightly aromatic character). When oxidizing the compounds all NICS values indicate an increased aromaticity.

Table S3. Results from above mentioned NICS calculation.

	1	2	3	4
MPO (***A***)	−8.91	−9.48	2.90	3.79
MPO (***B***)	−9.95	−9.87	−2.57	−2.20
MPO (***C***)	−10.77	−10.61	−10.15	−10.07
MPT (***A***)	−9.86	−10.23	−1.41	0.56
MPT (***B***)	−10.19	−9.96	−3.34	−2.75
MPT (***C***)	−12.02	−11.42	−10.46	−10.31

5.1 Detailed calculations on model compound 6a

Only in isomers **6a** and **6b** the phenoxazine units were aligned such that significant π-stacking interactions were possible. For both isomers the angle of the heteroaromatic ring as well as the intramolecular distance between the two phenoxazines was decreased with increasing oxidation of the molecule. **6a** was chosen for a more detailed theoretical investigation.

Table S4. Energies obtained for oxidation states ***A–C*** of isomer **6a** after geometry optimization and calculation of the harmonic vibrational frequencies (B3LYP-D3/def2-TZVP+COSMO). (Preoptimized groundstate ***A*** on the PBEh3c/def2-mSVP level of theory). In all calculations the COSMO solvation model (ε = 37.5, acetonitrile) was used. Single point energies were calculated on the PW6B95[14]-D3/def2-TZVP+COSMO level of theory.

	Oxidation state		
	A	***B***	***C***
E(PW6B95-D3) (E_h) [a]	−1461.8149236	−1461.645198134	−1461.450504813
ZPE (E_h) [b]	0.538759	0.5408906	0.5425405
G(298) (kcal mol^{-1}) [b]	297.70	300.05	300.59
Distance $d_{NO\text{-}Centroid}$ (Å)	3.745	3.468	3.330
Angle θ (°) [c]	158.8	174.1	177.8

[a] PW6B95-D3/def2-TZVP.

[b] B3LYP-D3/def2-TZVP.

[c] Average of both **MPO** units.

Table S5. Free energies of oxidation $\Delta G_{ox}(298)$ and oxidation potentials calculated from the energies listed in Table S2 (PW6B95-D3/def2-TZVP//B3LYP-D3/def2-TZVP+COSMO(CH_3CN)).

Oxidation process of **6a**	ΔG_{ox} (kcal mol^{-1})	E [a] (V)
A → ***B*** + e$^-$	110.2	−4.78
B → ***C*** + e$^-$	123.8	−5.37

[a] $E = -\Delta G_{ox}(298)/nF$

Table S6. Frontier molecular orbital energies (B3LYP-D3/def2-TZVP+COSMO) of **6a** in oxidation state ***A*** (uncharged), ***B*** (radical cation), and ***C*** (dication).

Molecular orbital	Energy of oxidation state (eV)		
	A	B_α / B_β	***C***
LUMO+1	−0.487	−1.174 / −1.090	−2.254
LUMO	−0.614	−1.483 / −1.372	−4.825
HOMO	−4.796	−5.367 / −4.150 (unoccupied)	−6.196
HOMO−1	−4.973	−5.846 / −5.292	−7.066
$gap_{HOMO/LUMO}$	+4.181	+1.143 (spin flip)	+1.371

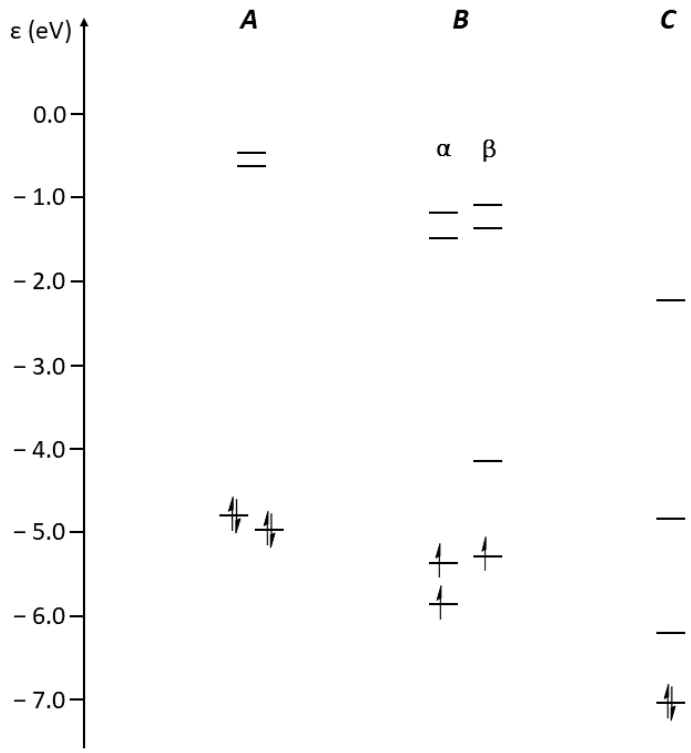

Figure S33. Frontier molecular orbital energies (B3LYP-D3/def2-TZVP+COSMO) of **6a** in oxidation state ***A*** (uncharged), ***B*** (radical cation), and ***C*** (dication).

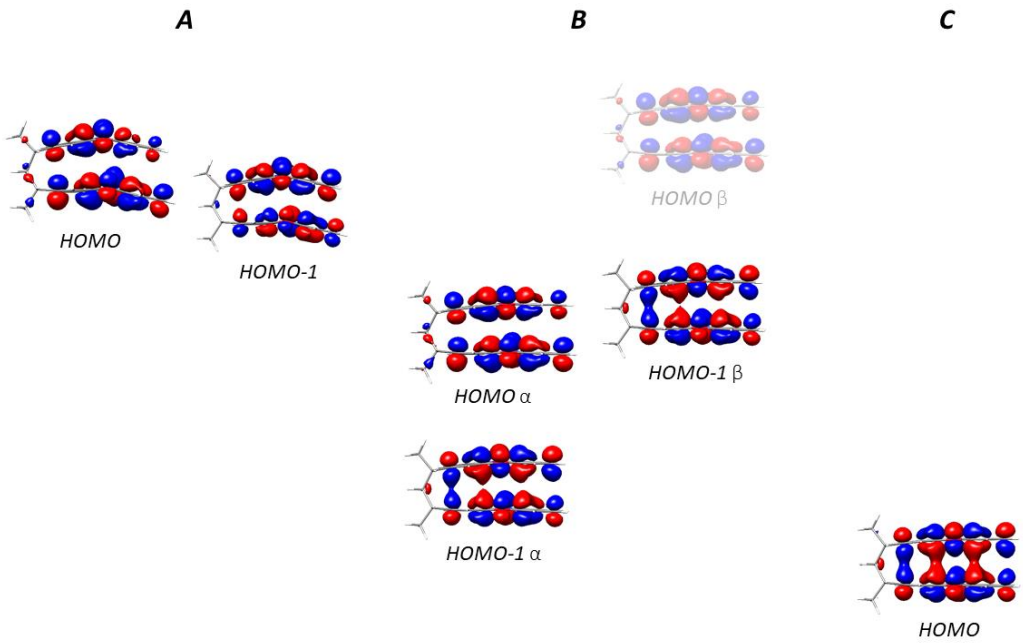

Figure S34. Highest occupied molecular orbitals (B3LYP-D3/def2-TZVP+COSMO) of **6a** in oxidation state ***A*** (uncharged), ***B*** (radical cation), and **C** (dication). In oxidation state ***B*** a large stabilisation of HOMO α and destabilisation of HOMO β is observed resulting in a shuffling of the frontier orbitals.

Table S7. Electrochemical data of **PVMPO** in comparison to values calculated for **6a**.

$E_{1/2,\,ox}$ (V) *vs.* Fc/Fc^+	$E_{HOMO,\,CV}$ (eV) [a]	$E_{g,\,opt}$ (eV) [b]	E_{LUMO} (eV) [c]	$E_{HOMO,\,calc}$ (eV) [d]	$E_{LUMO,\,calc}$ (eV) [d]	$E_{g,\,calc}$ (eV) [d]
0.09	−4.74	+3.41	−1.33	−4.80	−0.61	+4.18

[a] Calculated from the onset of the oxidation peak [$E_{HOMO} = -(E_{onset,\,ox} + 4.8)$ eV].[15]
[b] Optical band gap calculated from the onset of the longest wavelength absorption band (364 nm).
[c] $E_{LUMO} = E_{HOMO,\,CV} + E_{g,\,opt}$
[d] B3LYP-D3/def2-TZVP+COSMO.

5.2 Cartesian coordinates

5.2.1 Cartesian coordinates of 6a in oxidation State *A*

C	-1.3485683	5.2907429	-0.7650400
C	-0.3416939	4.1431397	-0.6031554
C	0.6548153	4.4683079	0.5268478
C	-1.0561982	2.8178700	-0.4218444
C	-1.8918055	2.5697151	0.6610808
C	-2.5009152	1.3301094	0.8421854
C	-2.3072303	0.2983234	-0.0755967
C	-1.4804943	0.5625055	-1.1723685
C	-0.8718901	1.7871970	-1.3438485
C	-2.2742631	-2.0254889	-0.6561791
C	-1.4421589	-1.7187020	-1.7434411
O	-1.2566947	-0.4063262	-2.1335048
C	-2.4493272	-3.3713590	-0.3322320
C	-1.8313361	-4.3707314	-1.0838887
C	-1.0147782	-4.0456048	-2.1540445
C	-0.8141702	-2.7042400	-2.4762378
C	1.9751607	3.6746983	0.5211043
C	2.9336163	4.2428905	1.5764262
C	1.7740278	2.1848887	0.7002613
C	1.1603969	1.6673019	1.8336302
C	0.8797699	0.3105066	1.9517842
C	1.1890275	-0.5736117	0.9195443
C	1.8529395	-0.0552459	-0.1974091
C	2.1510578	1.2883419	-0.3016434
C	1.5404719	-2.7830262	0.0741004
C	2.2000978	-2.2293722	-1.0340820
O	2.1580797	-0.8699062	-1.2716433
C	1.6008733	-4.1654720	0.2444344
C	2.2584599	-4.9694965	-0.6847528
C	2.8874571	-4.4061487	-1.7834868
C	2.8663339	-3.0206340	-1.9473211
N	-2.8850153	-0.9750576	0.0369875
C	-3.8073925	-1.2577802	1.1163917
N	0.8426210	-1.9289702	0.9289430
C	0.0435384	-2.4649798	2.0086681
H	-1.9150980	5.4470662	0.1558870
H	-0.8352393	6.2242514	-1.0058786
H	-2.0606948	5.0738701	-1.5633980
H	0.2317365	4.0741910	-1.5331178
H	0.9145293	5.5283572	0.4476409
H	0.1589683	4.3476331	1.4946835
H	-2.0547779	3.3362680	1.4082296
H	-3.1128239	1.1684965	1.7172835
H	-0.2210728	1.9202237	-2.1985018
H	-3.0623373	-3.6483389	0.5124500
H	-1.9832368	-5.4061460	-0.8077802
H	-0.5124873	-4.8165131	-2.7216530
H	-0.1668529	-2.4114225	-3.2919760
H	2.4357209	3.8233383	-0.4608296
H	3.1175983	5.3055218	1.4021797
H	2.5160782	4.1347801	2.5800307
H	3.8917363	3.7203946	1.5540418
H	0.8529047	2.3281625	2.6336167
H	0.3849323	-0.0493738	2.8413969
H	2.6267601	1.6411209	-1.2087365
H	1.1159479	-4.6250562	1.0925768
H	2.2705306	-6.0419386	-0.5386523
H	3.3965967	-5.0269856	-2.5086660
H	3.3476439	-2.5455874	-2.7926557
H	-4.4434554	-2.0959399	0.8404752
H	-4.4467734	-0.3936791	1.2810587
H	-3.2983232	-1.4997059	2.0573876
H	-0.7205992	-1.7410422	2.2822990
H	0.6372688	-2.7005068	2.9002459
H	-0.4599936	-3.3658249	1.6696920

5.2.2 Cartesian coordinates of 6a in oxidation State *B*

C	-1.4166842	5.1592301	-0.8655405
C	-0.3232040	4.0989518	-0.6662566
C	0.6260287	4.5234961	0.4715625
C	-0.9362896	2.7307790	-0.4578284
C	-1.7657467	2.4543088	0.6367791
C	-2.2951240	1.1953776	0.8494290
C	-2.0146013	0.1442472	-0.0346411
C	-1.1954685	0.4346410	-1.1431905
C	-0.6871201	1.7009233	-1.3572772
C	-2.0393609	-2.1597466	-0.7055694
C	-1.2288856	-1.8278319	-1.8060324
O	-0.8657390	-0.5298710	-2.0533565
C	-2.3515690	-3.5106763	-0.5079233
C	-1.8983258	-4.4740906	-1.3968670
C	-1.1153691	-4.1206604	-2.4910850
C	-0.7759583	-2.7895453	-2.6899113
C	1.9720016	3.7758262	0.5390897
C	2.8782821	4.4105572	1.6030196
C	1.7969367	2.2943403	0.7745171
C	1.1551868	1.8137300	1.9211028
C	0.8786673	0.4707171	2.0886107
C	1.2243807	-0.4579444	1.0985347
C	1.9351787	0.0250814	-0.0182118
C	2.2248490	1.3676137	-0.1690356
C	1.3882922	-2.6740736	0.2009631
C	2.1044742	-2.1559359	-0.8937925
O	2.3176316	-0.8115323	-1.0287404
C	1.2142255	-4.0599086	0.2710096
C	1.7112040	-4.8824798	-0.7274992
C	2.4078217	-4.3481676	-1.8084789
C	2.6101637	-2.9777234	-1.8854756
N	-2.4910667	-1.1456495	0.1335957
C	-3.4428628	-1.4466126	1.1967732
N	0.8852668	-1.7994137	1.1583772
C	0.0417697	-2.3106714	2.2296511
H	-2.0105550	5.2861085	0.0421537
H	-0.9700381	6.1239017	-1.1131052
H	-2.0922275	4.8754108	-1.6740675
H	0.2668051	4.0517392	-1.5861462
H	0.8496528	5.5854772	0.3396870
H	0.1090350	4.4371765	1.4316459
H	-1.9830884	3.2309455	1.3578796
H	-2.9000471	1.0207559	1.7249752
H	-0.0524350	1.8565147	-2.2196861
H	-2.9439943	-3.8112548	0.3417674
H	-2.1499019	-5.5112811	-1.2213579
H	-0.7589027	-4.8750885	-3.1781986
H	-0.1557484	-2.4794950	-3.5195959
H	2.4603410	3.8947654	-0.4324203
H	3.0444207	5.4665277	1.3815631
H	2.4269650	4.3417659	2.5950853
H	3.8474740	3.9104157	1.6371872
H	0.8331792	2.5042362	2.6887083
H	0.3705789	0.1471284	2.9829500
H	2.7305596	1.6842817	-1.0722973
H	0.6864458	-4.4981140	1.1028724
H	1.5522482	-5.9500105	-0.6584350
H	2.7915333	-4.9937435	-2.5866408
H	3.1454525	-2.5267314	-2.7103798
H	-4.0956365	-2.2522025	0.8774618
H	-4.0527119	-0.5717496	1.3937596
H	-2.9291971	-1.7411623	2.1145767
H	-0.5963269	-1.5167535	2.6005712
H	0.6391551	-2.7048449	3.0543489
H	-0.5920207	-3.1020051	1.8388358

5.2.3 Cartesian coordinates of 6a in oxidation State *C*

C	-1.4870692	5.1274072	-0.8382427
C	-0.3450851	4.1087979	-0.6899894
C	0.6091607	4.5401656	0.4405449
C	-0.8960581	2.7179616	-0.4928910
C	-1.6826650	2.3967229	0.6344792
C	-2.1639324	1.1279956	0.8492729
C	-1.8704768	0.0962087	-0.0611812
C	-1.0966883	0.4331894	-1.2035860
C	-0.6505713	1.7210276	-1.4254799
C	-1.9003396	-2.1772053	-0.7974668
C	-1.1306253	-1.8032890	-1.9228050
O	-0.7806278	-0.5047236	-2.1273302
C	-2.2323619	-3.5337399	-0.6468472
C	-1.8315078	-4.4515355	-1.5960021
C	-1.0846779	-4.0559550	-2.7111487
C	-0.7363766	-2.7269443	-2.8744982
C	1.9465988	3.7757674	0.4982053
C	2.8760825	4.4080531	1.5459007
C	1.7511520	2.3056064	0.7617529
C	1.1267754	1.8576510	1.9454897
C	0.8488054	0.5305374	2.1640823
C	1.1688065	-0.4302515	1.1871833
C	1.8615617	0.0245151	0.0323013
C	2.1641920	1.3577666	-0.1614980
C	1.2586928	-2.6525859	0.3191234
C	1.9613175	-2.1638593	-0.8073310
O	2.2246572	-0.8415313	-0.9402487
C	1.0255523	-4.0339800	0.3968075
C	1.4581791	-4.8662754	-0.6142546
C	2.1522790	-4.3579727	-1.7198462
C	2.4121018	-3.0042012	-1.8121399
N	-2.2931877	-1.1994406	0.0976266
C	-3.2004472	-1.5459387	1.1988373
N	0.8533260	-1.7605419	1.2966155
C	0.0977284	-2.2529098	2.4515160
H	-2.0629078	5.2115614	0.0854153
H	-1.0798771	6.1116896	-1.0737766
H	-2.1677594	4.8360412	-1.6391937
H	0.2250367	4.1032783	-1.6222629
H	0.8417293	5.5973979	0.2944859
H	0.0986956	4.4675292	1.4045898
H	-1.9003898	3.1606869	1.3676733
H	-2.7339985	0.9224556	1.7398979
H	-0.0581956	1.9133243	-2.3095933
H	-2.7918989	-3.8653702	0.2121559
H	-2.0903826	-5.4927955	-1.4640569
H	-0.7797989	-4.7857191	-3.4478245
H	-0.1552312	-2.3862676	-3.7198595
H	2.4239227	3.8703558	-0.4801277
H	3.0574653	5.4552043	1.2993252
H	2.4333039	4.3672806	2.5428496
H	3.8360691	3.8911117	1.5771501
H	0.8362528	2.5753264	2.6996456
H	0.3659530	0.2376974	3.0813112
H	2.6591571	1.6447802	-1.0793729
H	0.5114368	-4.4538954	1.2449766
H	1.2625304	-5.9270056	-0.5439725
H	2.4874628	-5.0246185	-2.5021599
H	2.9425439	-2.5751378	-2.6508367
H	-3.8568574	-2.3456315	0.8789979
H	-3.8012729	-0.6822163	1.4523587
H	-2.6302605	-1.8655921	2.0711954
H	-0.5194316	-1.4559206	2.8458831
H	0.7793177	-2.6066437	3.2232185
H	-0.5468858	-3.0653995	2.1349554

5.2.4 Cartesian coordinates of 6b in oxidation State *A*

C	-3.7065388	3.4772041	-1.6407245
C	-2.2730420	3.3201792	-1.1134936
C	-2.1369087	4.0431180	0.2399061
C	-1.8695995	1.8614265	-1.0554139
C	-2.4783525	0.9753101	-0.1758908
C	-2.0668724	-0.3492481	-0.0777033
C	-1.0099003	-0.8275374	-0.8505699
C	-0.4214664	0.0602343	-1.7576669
C	-0.8484938	1.3681493	-1.8702942
C	0.2643962	-2.6115393	-1.8081276
C	0.8436146	-1.6916188	-2.6958864
O	0.6589703	-0.3341277	-2.5246305
C	0.5135517	-3.9670211	-2.0212592
C	1.3462988	-4.3846567	-3.0578968
C	1.9241633	-3.4598575	-3.9132846
C	1.6555757	-2.1022461	-3.7334993
C	-0.7227275	4.1664333	0.8568062
C	0.2442534	4.8835150	-0.0856666
C	-0.1934958	2.8486956	1.3975907
C	-0.7651636	2.2766596	2.5294609
C	-0.3540702	1.0370584	3.0127301
C	0.6724402	0.3325106	2.3842623
C	1.2505558	0.9192745	1.2544803
C	0.8357437	2.1425618	0.7739068
C	1.8576146	-1.6934338	1.8975265
C	2.4097269	-1.0712515	0.7667866
O	2.2861048	0.2918008	0.5860391
C	2.0452224	-3.0688928	2.0374002
C	2.7758484	-3.7885755	1.0913911
C	3.3109655	-3.1545271	-0.0173436
C	3.1162723	-1.7835545	-0.1795614
N	-0.5005638	-2.1260668	-0.7482996
C	-1.0035247	-3.0275109	0.2651834
N	1.1573709	-0.9091977	2.8198794
C	0.6405728	-1.5040172	4.0344483
H	-3.9694905	4.5327187	-1.7414343
H	-3.8149585	3.0017883	-2.6173247
H	-4.4250600	3.0145328	-0.9601938
H	-1.6091792	3.8120255	-1.8289604
H	-2.5227488	5.0590462	0.1085715
H	-2.7946837	3.5595465	0.9668840
H	-3.2729056	1.3164162	0.4746972
H	-2.5622196	-1.0026438	0.6248070
H	-0.3345715	2.0180623	-2.5683841
H	0.0747272	-4.7044730	-1.3661102
H	1.5374327	-5.4422839	-3.1868087
H	2.5729523	-3.7792407	-4.7180724
H	2.0878281	-1.3515157	-4.3828370
H	-0.8559450	4.8175583	1.7277524
H	1.2044774	5.0644618	0.4007654
H	0.4359239	4.3126900	-0.9949286
H	-0.1713120	5.8476106	-0.3853790
H	-1.5683548	2.7923138	3.0427008
H	-0.8442698	0.6221937	3.8810986
H	1.3213107	2.5189054	-0.1143663
H	1.6154011	-3.5895395	2.8800983
H	2.9037973	-4.8549073	1.2260605
H	3.8551190	-3.7128373	-0.7664492
H	3.5036035	-1.2578665	-1.0418799
H	-0.2473471	-3.7741542	0.4896080
H	-1.9283958	-3.5325076	-0.0387090
H	-1.1955393	-2.4697555	1.1784834
H	-0.3046746	-2.0376641	3.8761123
H	0.4797168	-0.7265875	4.7775539
H	1.3708238	-2.2031439	4.4360590

5.2.5 Cartesian coordinates of 6c in oxidation State *A*

C	-2.3828218	3.4803820	3.4371537
C	-1.4899539	3.2968098	2.2039224
C	-0.0308217	3.6511366	2.5532541
C	-1.6348424	1.9137357	1.6028797
C	-1.4552161	0.7545542	2.3480889
C	-1.4952374	-0.5056712	1.7543489
C	-1.7373298	-0.6450689	0.3884542
C	-1.9274398	0.5275226	-0.3515664
C	-1.8833101	1.7717156	0.2375966
C	-1.6762323	-1.8895991	-1.6606931
C	-1.8591947	-0.6905103	-2.3690567
O	-2.1844724	0.4760276	-1.7087470
C	-1.3880340	-3.0388293	-2.3982858
C	-1.3158221	-2.9971751	-3.7901381
C	-1.5043783	-1.8048190	-4.4702142
C	-1.7679384	-0.6412369	-3.7453255
C	0.9403550	3.8331039	1.3725915
C	2.2537451	4.4554203	1.8717236
C	1.2215846	2.5667240	0.5906245
C	1.1269113	2.5319313	-0.7930344
C	1.3490964	1.3575251	-1.5130892
C	1.6944636	0.1781162	-0.8586227
C	1.8006271	0.2263008	0.5379610
C	1.5786121	1.3849784	1.2449652
C	1.8786216	-2.2097254	-0.7581153
C	1.9743540	-2.1218106	0.6403121
O	2.1514382	-0.9009902	1.2577202
C	1.7393179	-3.4804267	-1.3183863
C	1.7259567	-4.6194290	-0.5144139
C	1.8266430	-4.5111686	0.8634777
C	1.9412665	-3.2455869	1.4411086
N	-1.8064567	-1.8780452	-0.2722660
C	-1.7451856	-3.1147162	0.4813225
N	1.9414572	-1.0369041	-1.5102388
C	1.9597087	-1.0927218	-2.9586012
H	-2.3402918	4.5121206	3.7926161
H	-2.0626457	2.8330438	4.2565788
H	-3.4219188	3.2392099	3.2060303
H	-1.8221412	4.0124737	1.4448108
H	-0.0464913	4.5949947	3.1065131
H	0.3641025	2.9024222	3.2468695
H	-1.2403229	0.8162187	3.4073064
H	-1.3124494	-1.3791991	2.3620973
H	-2.0138014	2.6417890	-0.3929700
H	-1.2078218	-3.9721652	-1.8886467
H	-1.0959140	-3.9074584	-4.3328775
H	-1.4411125	-1.7655906	-5.5494421
H	-1.9162811	0.3098109	-4.2405973
H	0.4800168	4.5428072	0.6773134
H	2.9427141	4.6256421	1.0425425
H	2.7469787	3.7925382	2.5870371
H	2.0687600	5.4109078	2.3679131
H	0.8343711	3.4254634	-1.3314152
H	1.2236027	1.3651623	-2.5854701
H	1.6585881	1.3413657	2.3226953
H	1.6296439	-3.5871666	-2.3861855
H	1.6218817	-5.5908445	-0.9803045
H	1.8084684	-5.3914773	1.4919755
H	2.0167169	-3.1202861	2.5136700
H	-2.2746060	-2.9874972	1.4230720
H	-0.7186963	-3.4268783	0.6910744
H	-2.2460330	-3.9030827	-0.0766499
H	2.4284447	-0.1903425	-3.3455758
H	0.9578964	-1.1835910	-3.3867370
H	2.5588699	-1.9419403	-3.2799549

5.2.6 Cartesian coordinates of 6d in oxidation State *A*

C	-0.3980395	4.1504812	2.9921599
C	-1.0443164	3.7545960	1.6644312
C	-0.3196756	4.4179905	0.4683243
C	-1.2359050	2.2548052	1.5006655
C	-0.8167620	1.3173952	2.4338833
C	-0.9633996	-0.0542002	2.2129890
C	-1.5528209	-0.5308667	1.0472908
C	-1.9836040	0.4220210	0.1132861
C	-1.8403824	1.7704021	0.3342510
C	-1.9715528	-2.2552162	-0.5637840
C	-2.3850986	-1.2711518	-1.4767462
O	-2.5903944	0.0293485	-1.0653477
C	-1.8241636	-3.5588796	-1.0400065
C	-2.1058402	-3.8713593	-2.3691828
C	-2.5155294	-2.8860628	-3.2534745
C	-2.6450659	-1.5728684	-2.7984143
C	1.1490380	4.0253200	0.2095568
C	1.7941749	5.0364621	-0.7471002
C	1.2919880	2.6042260	-0.2971048
C	0.8448113	2.2148960	-1.5541404
C	0.9034481	0.8857781	-1.9682280
C	1.4344742	-0.0990797	-1.1365132
C	1.8917133	0.3042642	0.1230095
C	1.8278007	1.6183407	0.5313234
C	1.7183706	-2.3854517	-0.4724505
C	2.1646300	-1.9420869	0.7835566
O	2.4420617	-0.6088182	1.0030695
C	1.4941775	-3.7537144	-0.6328273
C	1.7346014	-4.6461758	0.4111945
C	2.1794907	-4.1887002	1.6411476
C	2.3849894	-2.8202489	1.8253440
N	-1.7448985	-1.8877901	0.7621535
C	-1.4368288	-2.8901797	1.7629089
N	1.5380182	-1.4502478	-1.4910938
C	1.1894952	-1.8809667	-2.8306297
H	-0.3087812	5.2365973	3.0533442
H	-0.9966971	3.8153379	3.8406545
H	0.6017516	3.7278539	3.1047633
H	-2.0482321	4.1969481	1.6606088
H	-0.8900352	4.2417079	-0.4468001
H	-0.3519755	5.4982386	0.6399071
H	-0.3302869	1.6324831	3.3457133
H	-0.5879406	-0.7466419	2.9515998
H	-2.1850367	2.4461719	-0.4371983
H	-1.4775415	-4.3361087	-0.3773079
H	-1.9862357	-4.8929843	-2.7061054
H	-2.7268716	-3.1220523	-4.2878480
H	-2.9587839	-0.7754387	-3.4599016
H	1.6892670	4.0845207	1.1576964
H	2.8336075	4.7723606	-0.9501531
H	1.2640289	5.0711343	-1.7014770
H	1.7720738	6.0402284	-0.3173434
H	0.4042022	2.9420787	-2.2243069
H	0.5098652	0.6192680	-2.9377691
H	2.1761664	1.8620812	1.5267470
H	1.1202091	-4.1296155	-1.5721112
H	1.5555211	-5.7017697	0.2525180
H	2.3596515	-4.8760548	2.4568494
H	2.7270037	-2.4241730	2.7729743
H	-1.7290216	-2.5183915	2.7429540
H	-0.3750496	-3.1485950	1.7839281
H	-2.0146448	-3.7897998	1.5630467
H	1.7224907	-2.8000427	-3.0649182
H	0.1165485	-2.0541109	-2.9491232
H	1.5057413	-1.1234931	-3.5444427

5.2.7 Cartesian coordinates of *N*-methylphenoxazine (MPO) in oxidation State *A*

H	1.4008823	4.5932617	-0.0673158
C	0.9309403	3.6289614	0.0729574
C	0.1241031	3.3874579	1.1740376
C	-0.4784494	2.1421084	1.3539645
C	-0.2998514	1.1251228	0.4154764
C	0.5272084	1.3873821	-0.6872805
C	1.1410838	2.6113171	-0.8589612
C	-0.2844104	-1.1912696	-0.1683103
C	0.5421420	-0.8892043	-1.2612172
O	0.7103737	0.4234371	-1.6612841
C	-0.4469725	-2.5336741	0.1758373
C	0.1702096	-3.5373949	-0.5711455
C	0.9760047	-3.2181050	-1.6530308
C	1.1702222	-1.8778360	-1.9909097
N	-0.9039662	-0.1339405	0.5076251
C	-1.8388206	-0.4105657	1.5803530
H	-0.0413582	4.1633067	1.9103657
H	-1.0907371	1.9717442	2.2269533
H	1.7675508	2.7633350	-1.7285868
H	-1.0582339	-2.8049299	1.0236700
H	0.0170347	-4.5715545	-0.2908921
H	1.4571821	-3.9948180	-2.2323279
H	1.7951729	-1.5917517	-2.8272214
H	-2.4692286	-1.2512185	1.3002117
H	-2.4806315	0.4544591	1.7302923
H	-1.3374507	-0.6456308	2.5267390

5.2.8 Cartesian coordinates of *N*-methylphenoxazine (MPO) in oxidation State *B*

H	1.1958608	4.6671929	-0.1933933
C	0.8129666	3.6728957	-0.0089556
C	-0.0513531	3.4425880	1.0714217
C	-0.5546932	2.1842076	1.3203708
C	-0.2009694	1.1077533	0.4870677
C	0.6871356	1.3589942	-0.5821681
C	1.1841831	2.6298965	-0.8349856
C	-0.1850938	-1.2082535	-0.0963678
C	0.7020919	-0.9117670	-1.1546086
O	1.0836946	0.3627678	-1.4102658
C	-0.5218944	-2.5553766	0.1274136
C	-0.0045337	-3.5392148	-0.6870207
C	0.8576363	-3.2192249	-1.7460926
C	1.2131084	-1.9048208	-1.9785389
N	-0.6824281	-0.1732056	0.6699833
C	-1.6972385	-0.4393651	1.6948227
H	-0.3273389	4.2604662	1.7225471
H	-1.2076068	2.0276340	2.1634012
H	1.8544237	2.7701753	-1.6719272
H	-1.1723747	-2.8249386	0.9434313
H	-0.2670156	-4.5714749	-0.5010134
H	1.2510899	-4.0024855	-2.3793255
H	1.8819666	-1.6235534	-2.7803452
H	-2.3170937	-1.2671925	1.3727394
H	-2.3219190	0.4375621	1.8116614
H	-1.2126044	-0.6812605	2.6401479

5.2.9 Cartesian coordinates of *N*-methylphenoxazine (MPO) in oxidation State *C*

H	1.1650337	4.6504591	-0.2170091
C	0.7994026	3.6497731	-0.0347772
C	-0.0960271	3.4240799	1.0454442
C	-0.5969863	2.1816751	1.3122448
C	-0.2050489	1.0937584	0.4981648
C	0.7184083	1.3467178	-0.5712373
C	1.2088922	2.6181599	-0.8420844
C	-0.1908829	-1.2027038	-0.0811184
C	0.7338331	-0.9067767	-1.1387815
O	1.1250576	0.3450141	-1.3406385
C	-0.5680473	-2.5514244	0.1163620
C	-0.0514628	-3.5121650	-0.7056662
C	0.8456612	-3.1874891	-1.7588944
C	1.2405523	-1.8914430	-1.9778744
N	-0.6515761	-0.1751069	0.6754225
C	-1.6522914	-0.4457870	1.7336310
H	-0.3857075	4.2566432	1.6701429
H	-1.2654912	2.0344673	2.1428604
H	1.8940357	2.7527983	-1.6665538
H	-1.2385901	-2.8245642	0.9127246
H	-0.3297896	-4.5448308	-0.5525413
H	1.2234683	-3.9772550	-2.3927852
H	1.9258309	-1.6102712	-2.7644090
H	-2.2551259	-1.2915163	1.4366781
H	-2.2819253	0.4249922	1.8472760
H	-1.1112235	-0.6572051	2.6534195

5.2.10 Cartesian coordinates of *N*-methylphenothiazine (MPT) in oxidation State *A*

H	1.4414870	4.6469046	0.2433456
C	0.9528923	3.6815770	0.2577474
C	0.1794035	3.2941915	1.3438744
C	-0.4391365	2.0475850	1.3648901
C	-0.3222239	1.1739224	0.2793907
C	0.4564292	1.5795258	-0.8170287
C	1.1015173	2.8100879	-0.8168282
C	-0.2788957	-1.1851111	-0.2776628
C	0.5041177	-1.0303682	-1.4335302
S	0.5379138	0.5406439	-2.2470985
C	-0.3564558	-2.4554111	0.3016759
C	0.3040773	-3.5389334	-0.2699605
C	1.0808623	-3.3728500	-1.4088331
C	1.1907090	-2.1081911	-1.9788410
N	-0.9639266	-0.0789358	0.2600178
C	-1.9945735	-0.3327803	1.2549773
H	0.0610914	3.9556086	2.1926838
H	-1.0141093	1.7608431	2.2327367
H	1.7055715	3.0909912	-1.6705453
H	-0.9339718	-2.6069506	1.2013311
H	0.2159699	-4.5136918	0.1926716
H	1.6013340	-4.2125512	-1.8502047
H	1.7969513	-1.9567551	-2.8632475
H	-2.6025778	-1.1732840	0.9277605
H	-2.6344637	0.5434377	1.3324932
H	-1.5899929	-0.5595050	2.2481846

5.2.11 Cartesian coordinates of *N*-methylphenothiazine (MPT) in oxidation State *B*

H	1.1009421	4.8352266	0.0676832
C	0.7520157	3.8151944	0.1520944
C	-0.0585708	3.4300414	1.2285833
C	-0.5136773	2.1356963	1.3420627
C	-0.1709242	1.1624034	0.3815994
C	0.6752784	1.5567618	-0.6830615
C	1.1178182	2.8816786	-0.7914184
C	-0.1270170	-1.2152950	-0.1797453
C	0.7220628	-1.0623417	-1.3025795
S	1.1884673	0.4772775	-1.9284309
C	-0.4260015	-2.5265256	0.2427419
C	0.0718443	-3.6169054	-0.4344153
C	0.8826444	-3.4517156	-1.5655854
C	1.2068525	-2.1827873	-1.9900958
N	-0.6624254	-0.1282649	0.4921633
C	-1.7848442	-0.3670607	1.4153235
H	-0.3274526	4.1520537	1.9876021
H	-1.1160005	1.8641800	2.1928250
H	1.7568893	3.1537513	-1.6211841
H	-1.0284111	-2.6848824	1.1215589
H	-0.1630746	-4.6109292	-0.0788270
H	1.2640163	-4.3136454	-2.0956842
H	1.8450619	-2.0329122	-2.8510429
H	-2.3764455	-1.1925913	1.0384094
H	-2.4077675	0.5187245	1.4429749
H	-1.4212809	-0.5971329	2.4164484

5.2.12 Cartesian coordinates of *N*-methylphenothiazine (MPT) in oxidation State *C*

H	1.0156802	4.8434167	-0.0205834
C	0.7060939	3.8134331	0.0868419
C	-0.1463415	3.4420088	1.1548610
C	-0.5767067	2.1540254	1.3138052
C	-0.1580266	1.1449704	0.4140820
C	0.7470709	1.5294516	-0.6374216
C	1.1503046	2.8691422	-0.7954796
C	-0.1157602	-1.2142948	-0.1435994
C	0.7940453	-1.0562849	-1.2482356
S	1.3722770	0.4388758	-1.7528047
C	-0.4922836	-2.5330900	0.2058174
C	-0.0187972	-3.5981134	-0.5089601
C	0.8379794	-3.4228343	-1.6227257
C	1.2424154	-2.1688887	-1.9854367
N	-0.6003415	-0.1397294	0.5445795
C	-1.6979929	-0.3888460	1.5186123
H	-0.4617819	4.1923129	1.8658495
H	-1.2070443	1.9118993	2.1506101
H	1.8170843	3.1224288	-1.6079359
H	-1.1240645	-2.7128264	1.0571018
H	-0.3020258	-4.5976765	-0.2112337
H	1.1823393	-4.2845688	-2.1768729
H	1.9120268	-2.0087304	-2.8190935
H	-2.2895298	-1.2200203	1.1648617
H	-2.3238570	0.4901139	1.5621837
H	-1.2627638	-0.6061750	2.4911769

6 Rate capability test and differential capacity plot of (X-)PVMPO-based composite electrodes

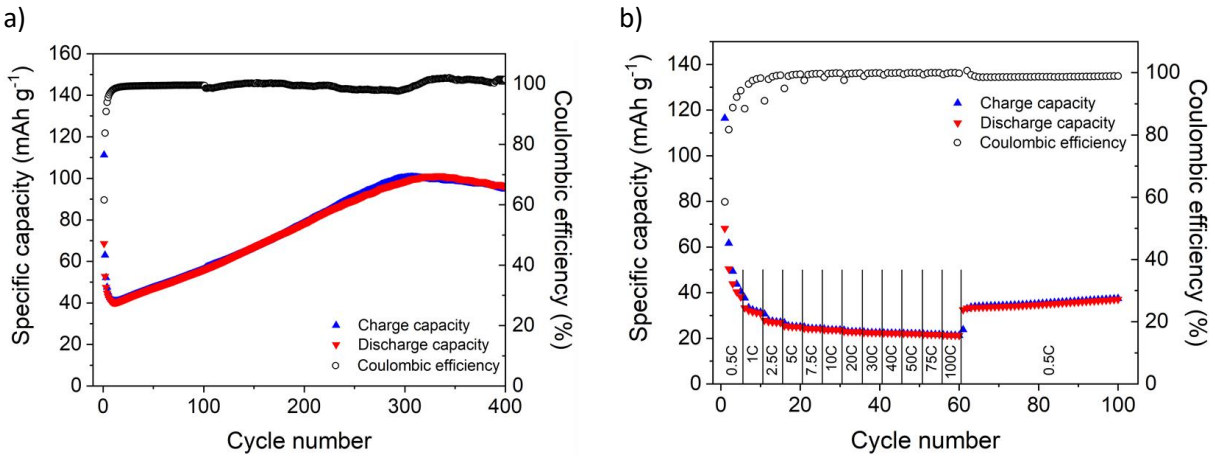

Figure S35. a) Constant current cycling at a 1C rate prior to a C-rate test (Figure 6A, Manuscript), and b) a C-rate test without previous constant current cycling of a **PVMPO**-based composite electrode (0.16 mg cm^{-2}).

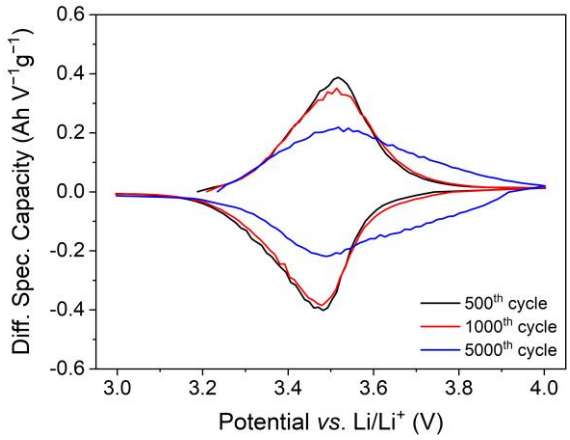

Figure S36. Differential capacity plot for selected cycles of the constant current cycling measurement (Figure 6C, Manuscript) of an **X-PVMPO**-based electrode at 100C rate.

7 Comparison of PVMPT, X-PVMPT, PVMPO and X-PVMPO

Table S8. Comparison of **PVMPT** and **X-PVMPT** from previous works[16,17] with the polymers **PVMPO** and **X-PVMPO** investigated in this work. Superior properties are highlighted in green.

	Previous work		**This work**	
	PVMPT	**X-PVMPT**	**PVMPO**	**X-PVMPO**
Structural formula	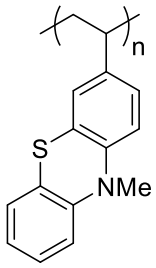	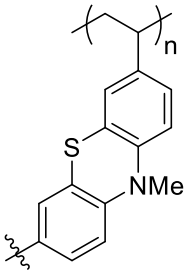	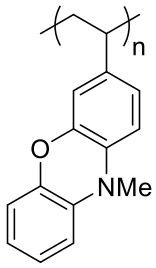	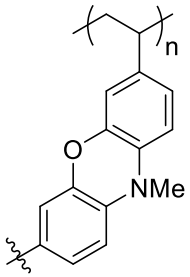
Molecular weight distribution (M_n)	2.4×10^4 g mol^{-1} (PDI of 2.0)	determination not possible due to cross-linked structure	2.4×10^4 g mol^{-1} (PDI of 1.7)	determination not possible due to cross-linked structure
Discharge potential (*vs.* Li/Li$^+$)	**3.5 V**	**3.5 V**	**3.5 V**	**3.5 V**
Specific capacity (th. spec. capacity)	up to **56 mAh g^{-1}** (112 mAh g^{-1})	up to **112 mAh g^{-1}** (112 mAh g^{-1})	up to **100 mAh g^{-1}** (120 mAh g^{-1})	up to **115 mAh g^{-1}** (120 mAh g^{-1})
Rate capability (cycling rate, capacity, percentage of capacity at 2.5C)	**high** **100C, 26 mAh g^{-1}, 46%**	**moderate** **up to 10C, 96 mAh g^{-1}, 94%** (no capacity accessible above 30C)	**high** **100C, 47 mAh g^{-1}, 55%**	**very high** **100C, 96 mAh g^{-1}, 83%**
Long term cycling stability (cycling rate, number of cycles, retained capacity, % capacity retention [a])	**10C, 10,000, 50 mAh g^{-1}, 93.5%**	1C, 1000, 102 mAh g^{-1}, 95%; **10C, 1000, 85 mAh g^{-1}, 100%**	**1C, 1000, 84 mAh g^{-1}, 84%**	1C, 1000, 79 mAh g^{-1}, 69% **100C, 10,000, 70 mAh g^{-1} 74%**
π-Interactions	Significant	Irrelevant or absent	Insignificant	Irrelevant or absent

[a] Capacity retention compared to maximum achieved capacity during cycling.

8 References

(1) Ahlrichs, R. TURBOMOLE V7.3, Forschungszentrum Karlsruhe GmbH, **2015**.

(2) Eichkorn, K.; Treutler, O.; Öhm, H.; Häser, M.; Ahlrichs, R. *Chem. Phys. Lett.* **1995**, *242* (6), 652–660.

(3) Weigend, F. *Phys. Chem. Chem. Phys.* **2006**, *8* (9), 1057–1065.

(4) Grimme, S.; Antony, J.; Ehrlich, S.; Krieg, H. *J. Chem. Phys.* **2010**, *132* (15), 154104.

(5) Grimme, S.; Ehrlich, S.; Goerigk, L. *J. Comput. Chem.* **2011**, *32* (7), 1456–1465.

(6) Becke, A. D.; Johnson, E. R. *J. Chem. Phys.* **2005**, *123* (15), 154101.

(7) Johnson, E. R.; Becke, A. D. *J. Chem. Phys.* **2006**, *124* (17), 174104.

(8) Grimme, S.; Brandenburg, J. G.; Bannwarth, C.; Hansen, A. *J. Chem. Phys.* **2015**, *143* (5), 054107.

(9) Becke, A. D. *J. Chem. Phys.* **1993**, *98* (7), 5648–5652.

(10) Stephens, P. J.; Devlin, F. J.; Chabalowski, C. F.; Frisch, M. J. *J. Phys. Chem.* **1994**, *98* (45), 11623–11627.

(11) Bühl, M.; van Wüllen, C. *Chem. Phys. Lett.* **1995**, *247* (1–2), 63–68.

(12) Schleyer, P. V. R.; Maerker, C.; Dransfeld, A.; Jiao, H.; Van Eikema Hommes, N. J. R. *J. Am. Chem. Soc.* **1996**, *118* (26), 6317–6318.

(13) Frisch, M. J.; Trucks, G. W.; Schlegel, H. B.; Scuseria, G. E.; Robb, M. A.; Cheeseman, J. R.; Scalmani, G.; Barone, V.; Petersson, G. A. ; Nakatsuji, H.; Li, X.; Caricato, M.; Marenich, A. V.; Bloino, J.; Janesko, B. G.; Gomperts, R.; Mennucci, B.; Hratchian, H. P.; Ortiz, J. V.; Izmaylov, A. F.; Sonnenberg, J. L.; Williams-Young, D.; Ding, F.; Lipparini, F.; Egidi, F.; Goings, J.; Peng, B.; Petrone, A.; Henderson, T.; Ranasinghe, D.; Zakrzewski, V. G.; Gao, J.; Rega, N.; Zheng, G.; Liang, W.; Hada, M.; Ehara, M.; Toyota, K.; Fukuda, R.; Hasegawa, J.; Ishida, M.; Nakajima, T.; Honda, Y.; Kitao, O.; Nakai, H.; Vreven, T.; Throssell, K.; Montgomery, Jr., J. A.; Peralta, J. E.; Ogliaro, F.; Bearpark, M. J.; Heyd, J. J.; Brothers, E. N.; Kudin, K. N.; Staroverov, V. N.; Keith, T. A.; Kobayashi, R.; Normand, J.; Raghavachari, K.; Rendell, A. P.; Burant, J. C.; Iyengar, S. S.; Tomasi, J.; Cossi, M.; Millam, J. M.; Klene, M.; Adamo, C.; Cammi, R.; Ochterski, J. W.; Martin, R. L.; Morokuma, K.; Farkas, O.; Foresman, J. B.; Fox, D. J. Gaussian 16, Gaussian, Inc., Wallingford CT, **2019**.

(14) Zhao, Y.; Truhlar, D. G. *J. Phys. Chem. A* **2005**, *109* (25), 5656–5667.

(15) D'Andrade, B. W.; Datta, S.; Forrest, S. R.; Djurovich, P.; Polikarpov, E.; Thompson, M. E. *Org. Electron.* **2005**, *6* (1), 11–20.

(16) Kolek, M.; Otteny, F.; Schmidt, P.; Mück-Lichtenfeld, C.; Einholz, C.; Becking, J.; Schleicher, E.; Winter, M.; Bieker, P.; Esser, B. *Energy Environ. Sci.* **2017**, *10* (11), 2334–2341.

(17) Otteny, F.; Kolek, M.; Becking, J.; Winter, M.; Bieker, P.; Esser, B. *Adv. Energy Mater.* **2018**, *8* (33), 1802151.